

# On Dust in the Early Universe

Takaya Nozawa

(IPMU, University of Tokyo)

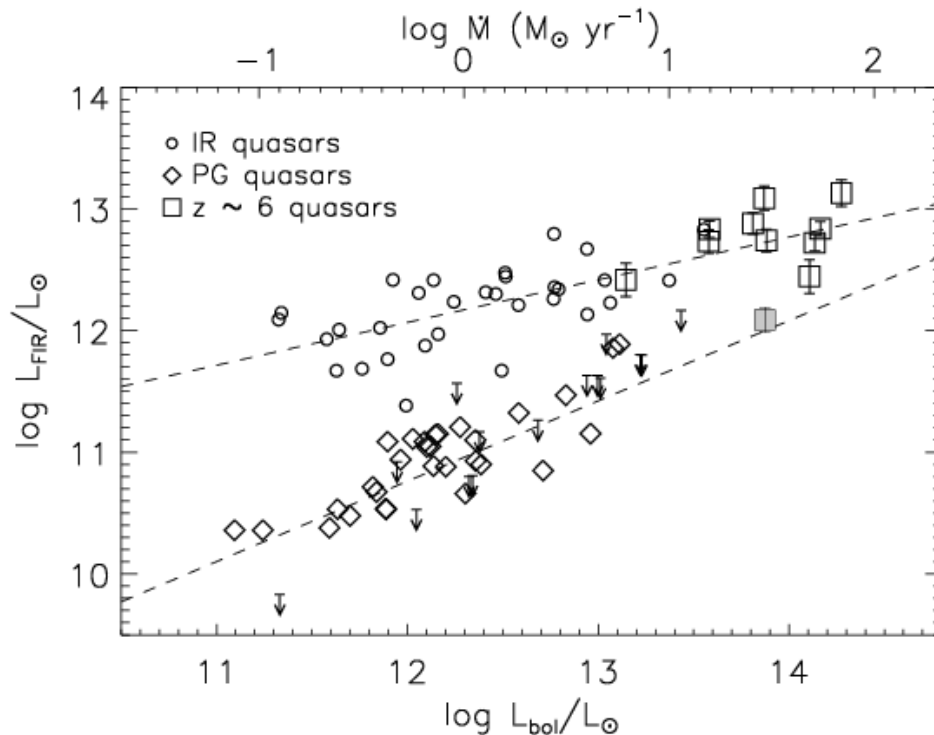
## Contents:

1. Observations of dust at high- $z$
2. Formation of dust in supernovae
3. Critical metallicity
4. EMP-stars and dust

# **1. Observations of dust at high- $z$**

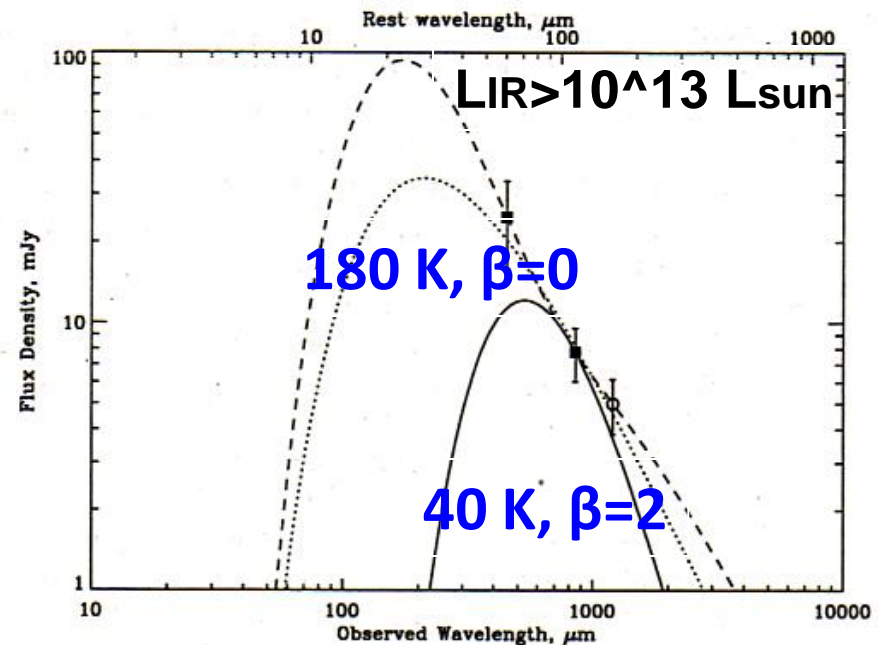
# 1-1. Discovery of large amounts of dust at $z > 5$

- The submm observations have confirmed the presence of dust in excess of  $10^8 M_{\text{sun}}$  in 30% of  $z > 5$  quasars
  - We see warm dust grains heated by absorbing stellar lights in the host galaxies of the quasars



Wang+08, ApJ, 687, 848

SDSS J1148+5251 at  $z=6.4$



Robson+04, MNRAS, 351, L29

# 1-2. What are sources of dust in $z = 6.4$ quasar?

## ▪ Type II SNe arising from short-lived massive stars

- $\sim 0.1 M_{\text{sun}}$  per SN (Maiolino+06, MmSAI, 77, 643)
- $> 1 M_{\text{sun}}$  per SN (Dwek+07, ApJ, 662, 927)
- sufficient only with SN-dust (Li+08, ApJ, 678, 41)

## ▪ AGB stars are more dominant than SNe (50-80 %)

(Valiante+09, MNRAS, 397, 1661)

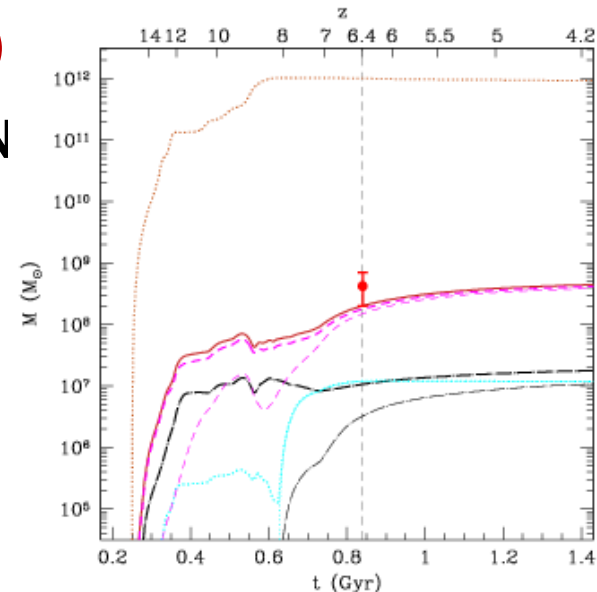
→  $\sim 0.01 M_{\text{sun}}$  per AGB,  $\sim 0.05 M_{\text{sun}}$  per SN

## ▪ grain growth in the ISM

(Draine 2009, arXiv:0903.1658)

## ▪ quasar outflow

(Elvis+02, ApJ, 567, L107)

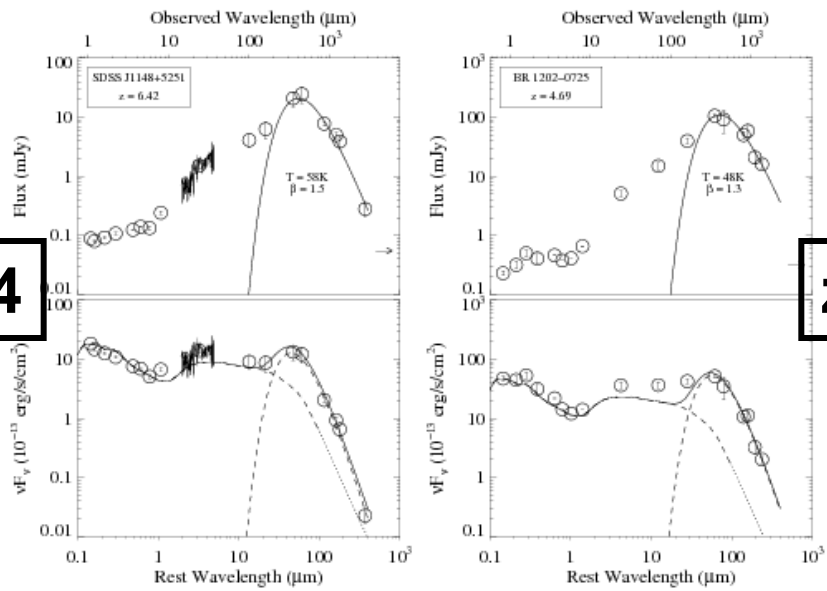


# 1-3. Herschel Observations of z=6.4 quasar

**Leipski+10**  
**(arXiv:1005.5016)**

**z=6.4**

**z=4.7**



- \*Herschel (3.5m)**
- PACS :  
70, 100, 160 μm
  - SPIRE  
250, 350, 500 μm

**Fig. 3.** Spectral flux distributions (*top*) and spectral energy distributions (*bottom*) for J1148+5251 (*left*) and for 1202–0725 (*right*). The arrow indicates the level of the 1.4 GHz (observed frame) radio emission (Tab. 1). In the top plot the solid line shows a single temperature grey body fit to the data at  $\lambda_{\text{obs}} > 160 \mu\text{m}$ . In the bottom panels we show as dashed lines the same greybody and also the mean SED for optically-luminous SDSS QSOs (Richards et al. 2006), scaled to the 1450 Å (rest frame) data point. The mean SED was extrapolated for wavelengths longer than 100 μm (rest frame) assuming  $F_{\nu} \sim \nu^2$  (dotted line). The solid line is the sum of the scaled SED and the fitted greybody. Both objects clearly show a large excess of cold dust emission ( $\lambda \gtrsim 30 \mu\text{m}$ , rest frame) compared to the mean QSO template. For J1148+5251 we here also include a *Spitzer*/IRS spectrum, which we retrieved from the archive and processed in a standard manner.

- a broad range of dust temperature ( $L_{\text{IR}} > 10^{14} L_{\text{sun}}$ )
- Another source northwest of the QSO J1148+5251 at z=6.4 is clearly visible

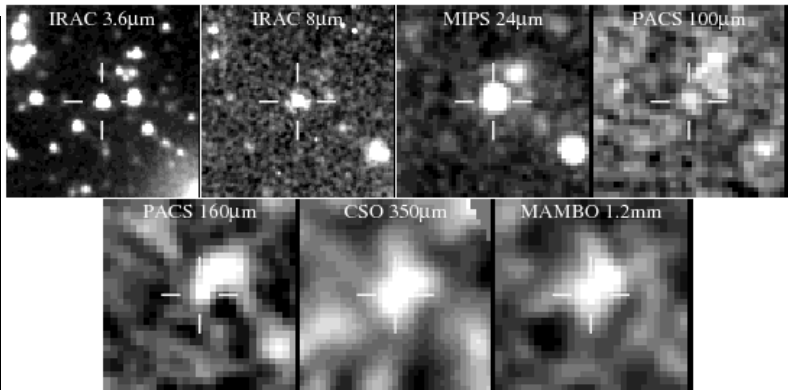


**Fig. 1.** Infrared and (sub)mm images of J1148+5251. All images are 60'' wide and north is up with east to the left. Another nearby source northwest of the QSO (see text) is clearly visible at longer wavelengths.

# 1-4. Sources of dust in $5 < z < 6.4$

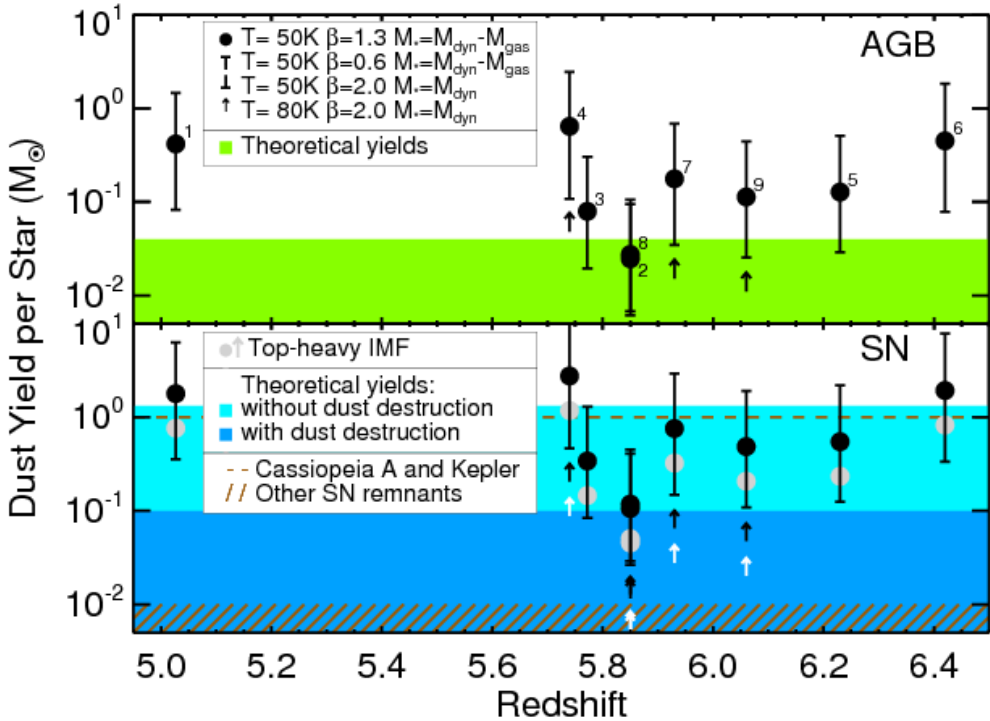


**Fig. 1.** Dust yields per AGB star (*top*) or per SN (*bottom*) required to explain dust in the  $z > 5$  QSOs. For reasonable assumptions on the dust properties, AGB stars are not efficient enough and SNe would need to be unfeasibly efficient to form dust in these sources suggesting rapid grain growth in the ISM is likely to be responsible for the large dust masses. *Circles:* the best estimates of the required dust yields with error bars reflecting the uncertainty of  $\beta$  and  $M_*$ . Numbers indicate the QSOs as in Tab. 1. *Arrows:* strict and unlikely lower limits with very high  $T_{\text{dust}}$  and  $\beta$  shown where data allow it (Tab. 1). *Gray symbols* indicate that a top-heavy IMF was adopted. *Dashed line and diagonal lines:* the dust yields derived for Cassiopeia A, Kepler ( $\sim 1 M_{\odot}$ ) and other SN remnants ( $\sim 10^{-3}$ – $10^{-2} M_{\odot}$ ), respectively. *Green area:* theoretical dust yields for AGB stars ( $\lesssim 4 \cdot 10^{-2} M_{\odot}$ ). *Light blue and blue areas:* theoretical SN dust yields without ( $\lesssim 1.32 M_{\odot}$ ) and with dust destruction implemented ( $\lesssim 0.1 M_{\odot}$ ), respectively.

Grain growth in the ISM is required for at least 3 out of 9 QSOs at  $z > 5$

Michalowski+10  
(arXiv:1006.5466)

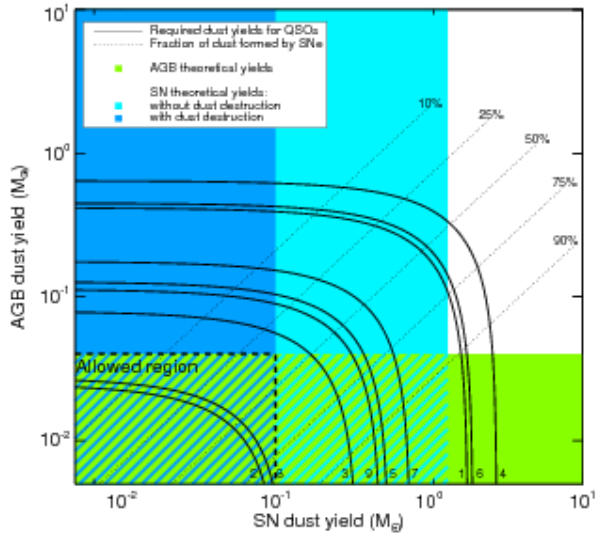
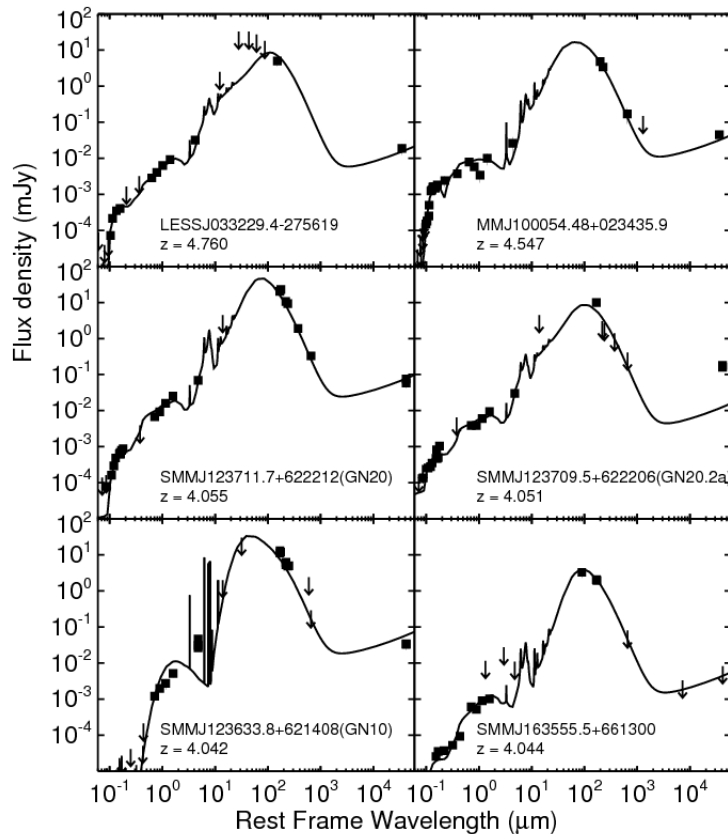


**Fig. 2.** The relation of the required dust yields per AGB star and per SN for different fractions of dust formed by SNe (shown as *dotted lines*). This is a combination of panels in Fig. 1 relaxing the assumption that only AGB stars or only SNe produced dust in the  $z > 5$  QSOs. The theoretically allowed regions of dust yields are shown as in Fig. 1. *Hashed region outlined by the dashed line* corresponds to the allowed region, where the dust yields for both AGB stars and SNe are within theoretical limits (with the dust destruction implemented). The *solid lines* correspond to the  $z > 5$  QSOs numbered as in Tab. 1. If higher fraction of dust is attributed to SNe then the QSOs move towards bottom-right corner. The combined effort of AGB stars and SNe can explain dust in QSO 2 and 8, but not in QSO 1, 4 and 6. Dust in QSOs 3, 5, 7 and 9 may have been formed by these stellar sources, but only if little dust is destroyed in SN shocks and that SN account for more than 50–75% of dust in these QSOs.

# 1-5. Dust production in submm galaxies at $z > 4$



**Michalowski+10, ApJ, 712, 942**

## Population synthesis (GRASIL)

- average SFR :  $\sim 2500 M_{\text{sun}}/\text{yr}$
- stellar mass :  $\sim 3.6 \times 10^{11} M_{\text{sun}}$
- dust mass :  $\sim 6.7 \times 10^8 M_{\text{sun}}$
- gas-to dust ratio :  $\sim 60$

## Dominant dust sources

- AGB stars for three
- SNe ( $0.15\text{-}0.65 M_{\text{sun}}$ ) for three

TABLE 5  
DUST YIELDS PER STAR REQUIRED TO EXPLAIN DUST IN  $z > 4$  SMGs

Dust Producer	IMF	Total Mass	Dust Yields ( $M_{\odot}$ Per Star)					
			LESS	MM	GN20	GN20.2a	GN10	SMM
AGB ( $2.5 < M < 8M_{\odot}$ )	Salpeter	$M_*$	0.03	0.06	0.04	0.17	0.05	0.07
AGB ( $2.5 < M < 8M_{\odot}$ )	Salpeter	$M_* - M_{\text{burst}}$	0.04	0.31	0.06	0.20	$\infty$	0.09
SN ( $M > 8M_{\odot}$ )	Salpeter	$M_*$	0.14	0.22	0.15	0.65	0.18	0.27
SN ( $M > 8M_{\odot}$ )	Top-heavy	$M_*$	0.05	0.08	0.05	0.23	0.06	0.10

NOTE. — The IMF is either Salpeter (1955) with  $\alpha = 2.35$  or top-heavy with  $\alpha = 1.5$ . The total mass indicates if the entire stellar mass ( $M_*$ ) was used to calculate the number of stars (Equation A1), or if stars created during the ongoing starburst were excluded ( $M_* - M_{\text{burst}}$ ). The last six columns contain dust yields for all SMGs in the order given in Table 3. Only the first parts of their names are given for brevity.



# 1-6. Dust mass in submm galaxies at $2 < z < 4$

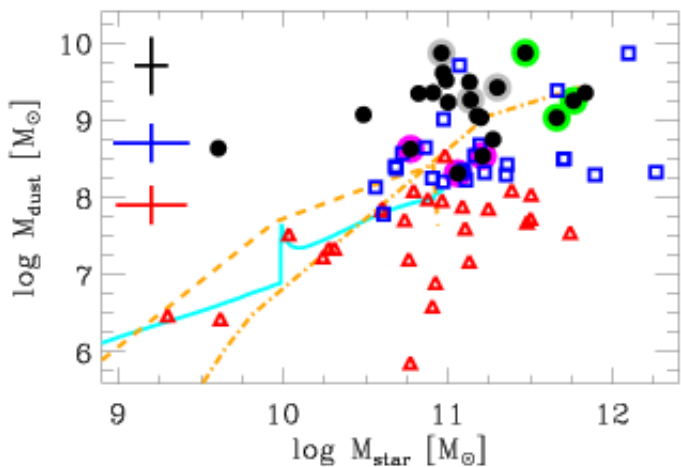


**Fig. 1.** Stellar mass versus dust mass. Blue squares show local ULIRGs, red triangles refer to local spirals, while black circles correspond to high- $z$  SMGs. Large gray, magenta and green circles mark respectively photo- $z$ , the triple image in Abell2218 and blended SMG systems. Median  $1\sigma$  error bars for the different samples (same color code) are shown on the left. The solid cyan and dashed (dot-dashed) orange lines show the predictions of Calura et al. (2008) model for spirals and proto-ellipticals with mass of  $10^{11}$  ( $10^{12}$ )  $M_{\odot}$ .

## Santini+10 (arXiv:1005.5678) using Herschel/PACS and GRASIL

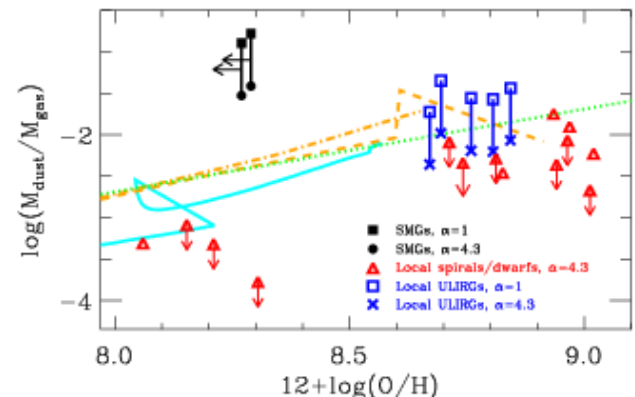


**Fig. 3.** Dust-to-gas ratio versus metallicity. The black and blue symbols show high- $z$  SMGs and local ULIRGs, respectively, by assuming different conversion factors as indicated by the legend. Red triangles refer to local spirals. The green dotted line shows the trend expected by Eq. 1. The solid cyan and dashed (dot-dashed) orange lines show the evolutionary tracks predicted by the model of Calura et al. (2008) for spirals and proto-ellipticals with mass of  $10^{11}$  ( $10^{12}$ )  $M_{\odot}$ .

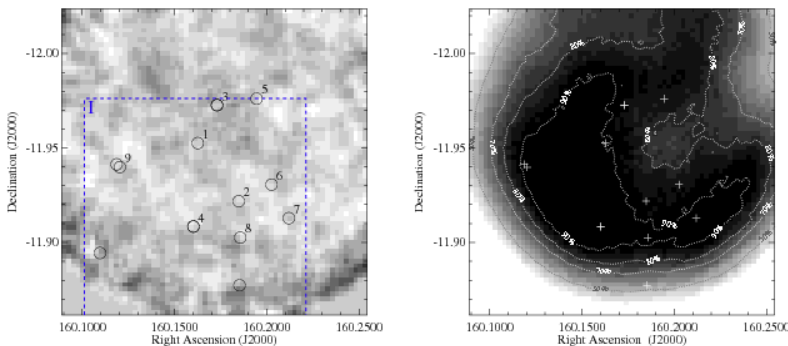


**Figure 1.** Our LABOCA map (left, smoothed by convolution with the  $19''$  beam) and associated coverage map (right). The dashed line denotes the region within which we have existing optical data and circles mark the optical locations of spectroscopically-confirmed  $z \sim 5$  Lyman break galaxies. Each circle matches the beam FWHM for an unresolved source. Numbered circles indicate sources used in the stacking analysis. Colour is inverted so black indicates a high-flux signal.

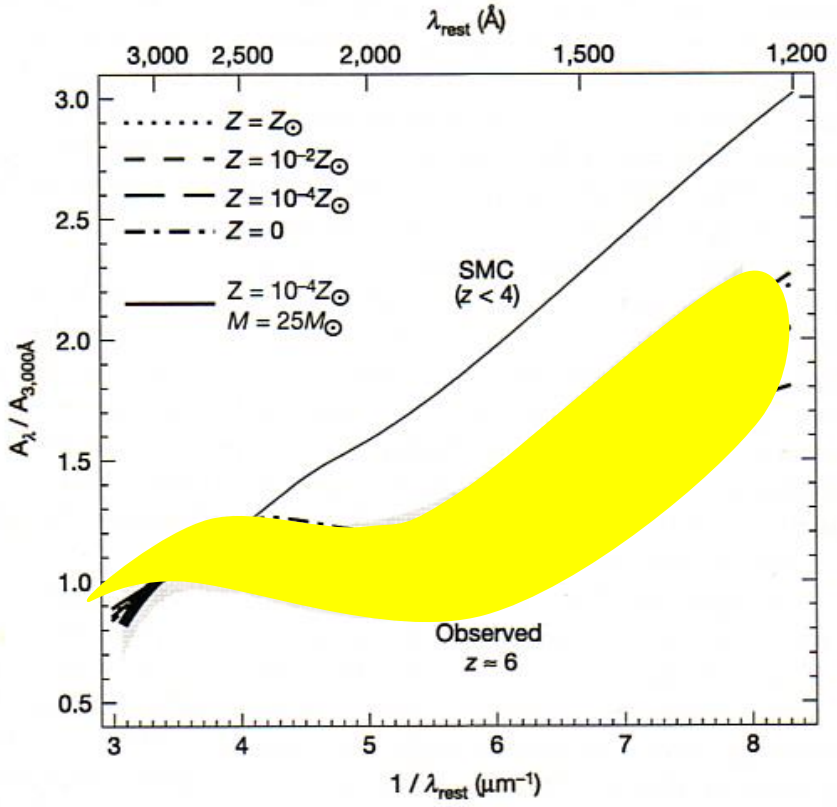
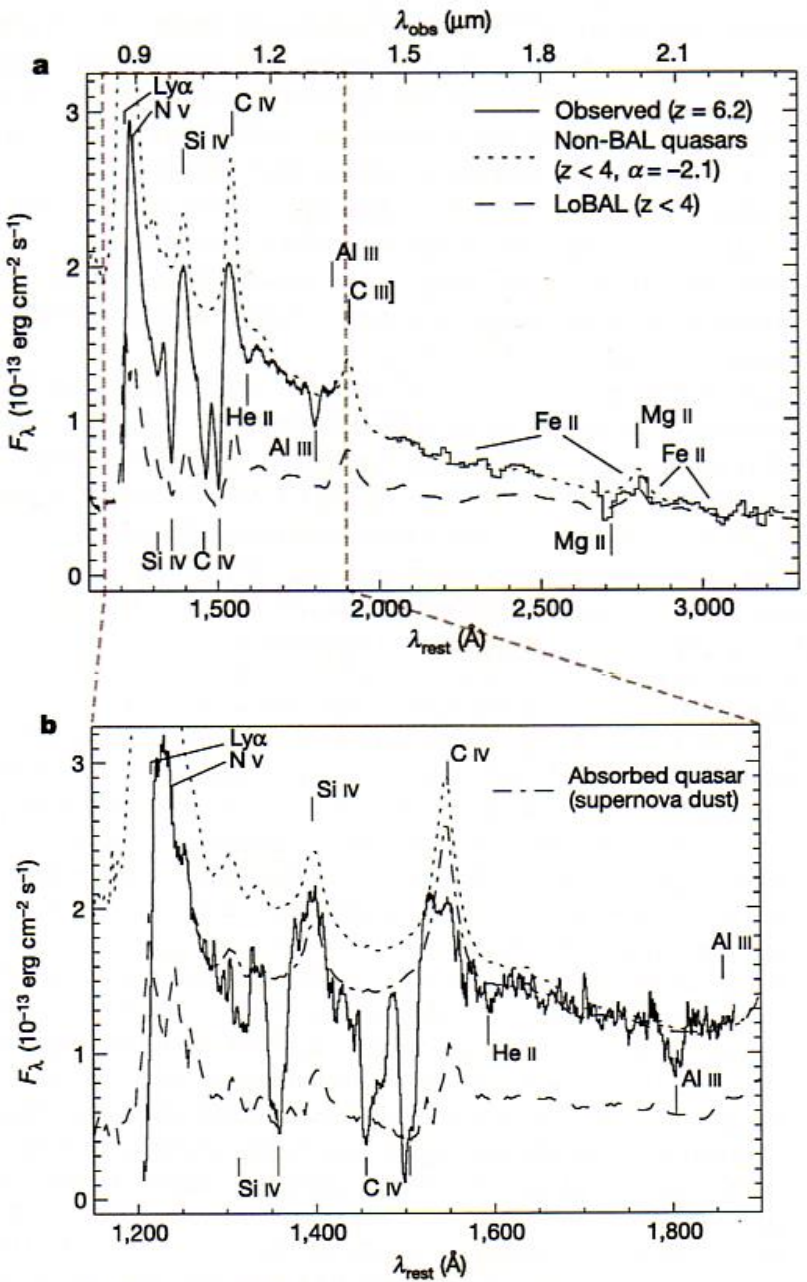
▪ overdense region of LBGs (9 objects) at  $z=5.16$   
**Non-detection at  $870 \mu\text{m}$**   
 **$\rightarrow M_{\text{dust}} < 1.2 \times 10^8 M_{\text{sun}}$**

## Stanway+10 (arXiv:1007.0440)



# 1-7. Extinction curves at high-z quasars

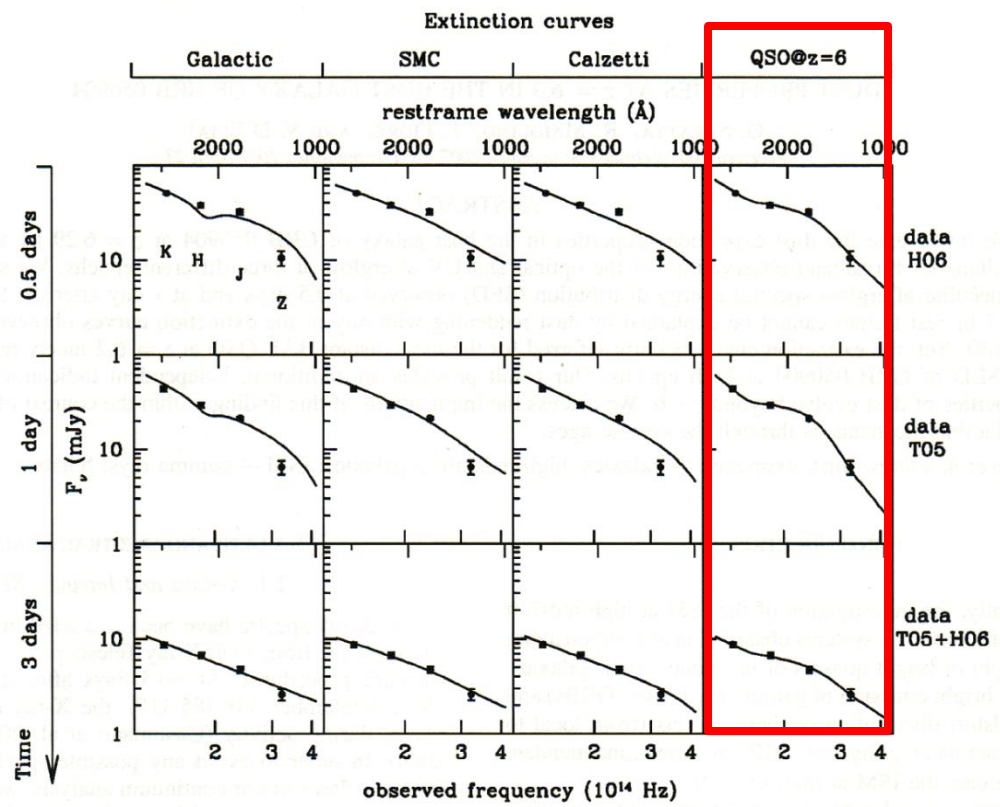
**Maiolino+04, Nature, 431, 533**  
**SDSS J1048+4637 at z=6.2**  
 Broad absorption line (BAL) quasars



**different dust properties from those at low redshifts**

# 1-8. Extinction curves from high-z GRBs

## GRB 050904 at z=6.3



**Stratta+07, ApJ, 661, L9**

## GRB 071025 at z~5

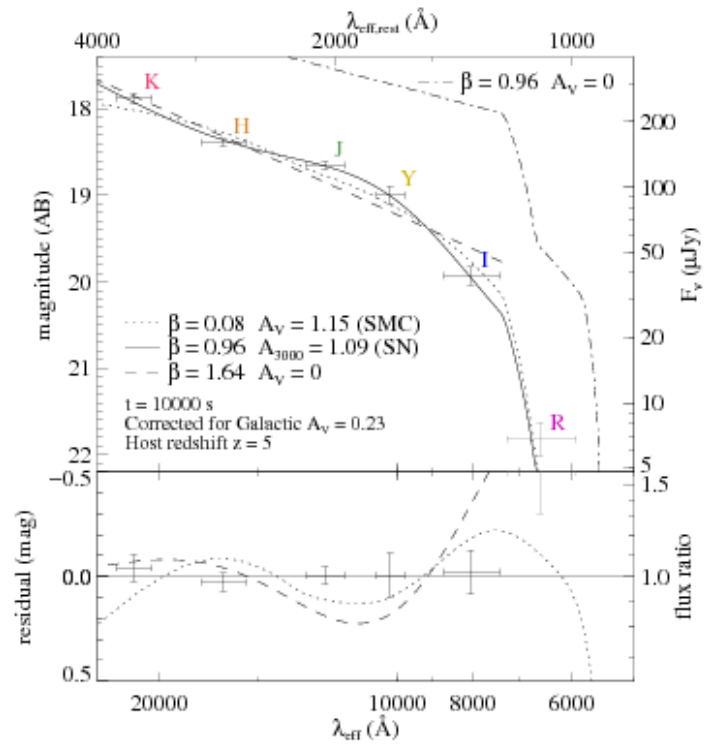
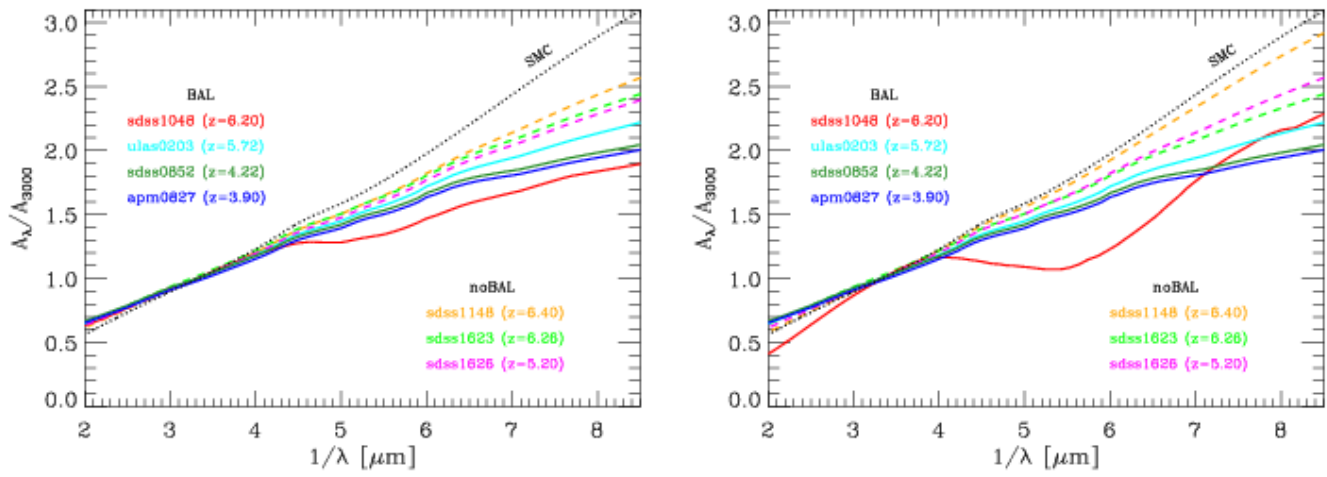


**Figure 3.** Spectral energy distribution of GRB 071025 inferred from our broadband photometry, fit with different extinction models. Note the spectral flattening between *J* and *H* that contrasts with red *H* – *K* and *I* – *Y* colours. (The *R* – *I* colour is due to absorption by the Lyman- $\alpha$  forest.) Traditional models (such as SMC-like extinction, shown here as a dotted line) cannot reproduce this feature and give poor fit residuals ( $\chi^2/\text{dof} = 20.8/2$ ). The supernova-dust model of Maiolino et al. (2004), shown as the solid line, is an excellent fit ( $\chi^2/\text{dof} = 0.81/2$ ). The dot-dashed line represents the intrinsic afterglow SED (for the SN model) without extinction applied but including our model of the IGM opacity at this redshift.

**additional evidence for different dust properties at high-z ( $z > 5$ ) but see Zafar+10, A&A, 514, 94**

**Perley+09 (arXiv:0912.2999)**

# 1-9. Extinction curves at $3.9 < z < 6.4$



**Gallerani+10**  
(arXiv:1006.4463)

**7 of 33 requires substantial dust extinction, which deviates from the SMC**

Fig. 4. Best fit extinction curves of reddened quasars. The solid lines are for BAL quasars, while dashed lines are for non-BAL quasars. For comparison the SMC extinction curve is also shown and labeled in the Figure (dotted black line). The panel on the left shows the results assuming a minimum intrinsic slope  $\alpha_{\lambda, \text{min}} = -2.9$ , while the panel on the right is obtained with  $\alpha_{\lambda, \text{min}} = -2.6$ .

**The mean Extinction curves for BAL quasars deviates from the SMC with level > 95 %**

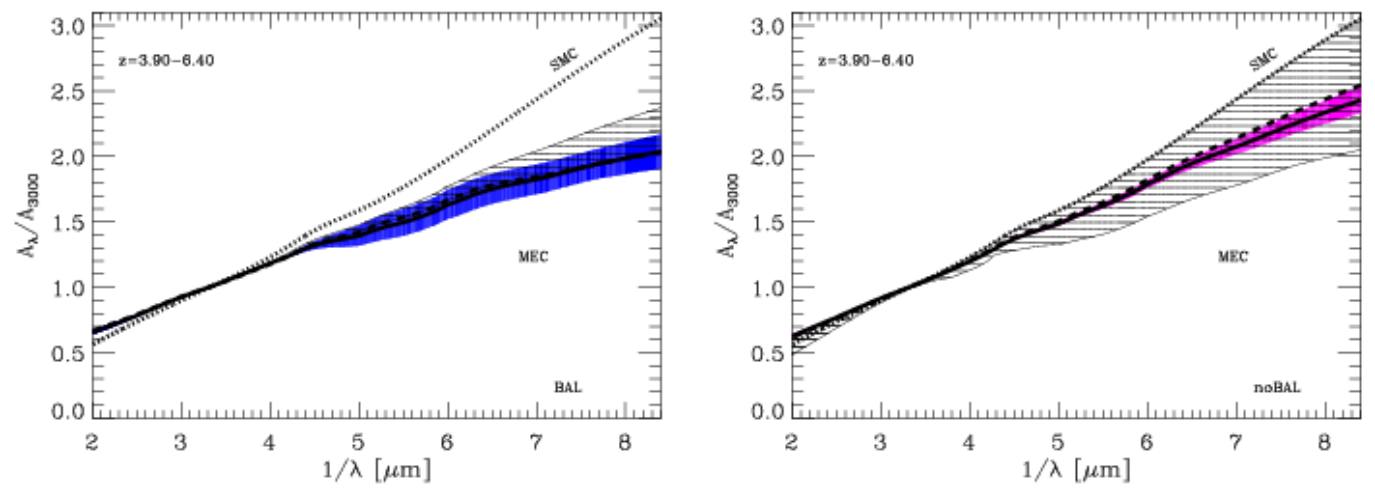


Fig. 6. Mean (MEC) and simultaneous/global (GEC) extinction curve of reddened quasars divided into BAL (left) and non-BAL (right). The coding is the same as in Fig. 5.

# 1-10. Concluding remarks

- **what are the main sources of a huge amount dust grains at  $z > 4$** 
  - SNe? AGB stars? grain growth in the ISM?  
quasar outflow? mass-loss winds of massive stars?  
**how about PISNe? any other sources?**
- **Properties of dust at high- $z$  are likely to be different from those at low- $z$** 
  - Is there really no extinction in many high- $z$  quasar systems?
- **Are there massive dust in primeval galaxies such as LBGs?**

## **2. Formation of dust in SNe**

# 2-1. Theory vs. Observation

## SNe are important sources of interstellar dust?

### • Theoretical studies

- before destruction : 0.08-2  $M_{\text{sun}}$  in Type II-P SNe  
(Todini & Ferrara 2001; Nozawa et al. 2003)
- after destruction :  
0.01-0.1  $M_{\text{sun}}$  (Bianchi & Schneider 2007)  
0.08-0.8  $M_{\text{sun}}$  (Nozawa et al. 2007)

### • Observational works

- IR observations of dust-forming SNe :  $< 10^{-2} M_{\text{sun}}$   
(e.g., Meikle et al. 2007, Kotak et al. 2009)
- submm observations of SNRs :  $\sim 1 M_{\text{sun}}$   
(Dunne et al. 2003; Morgan et al. 2003)
- FIR observation of Cas A : 0.03-0.075  $M_{\text{sun}}$   
(Sibthorpe et al. 2009; Barlow et al. 2010)



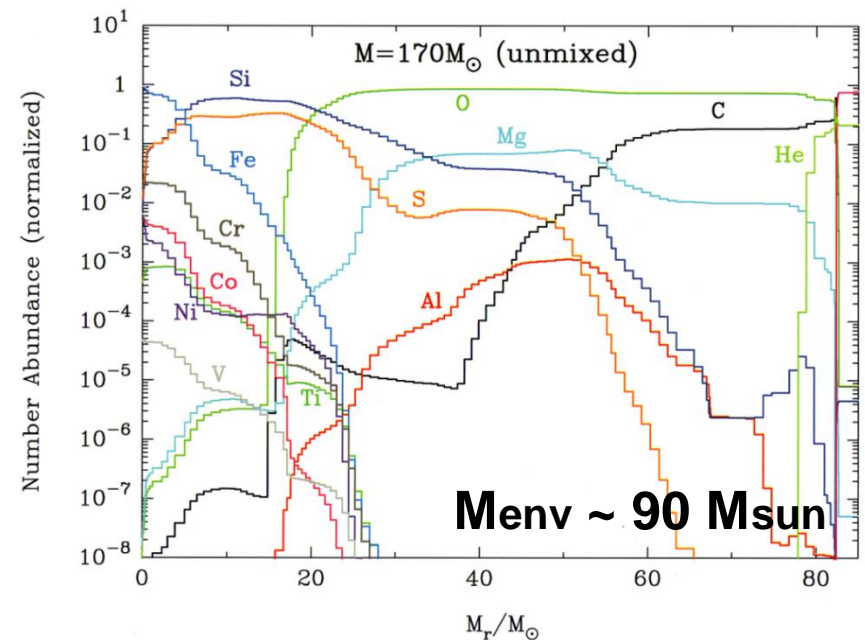
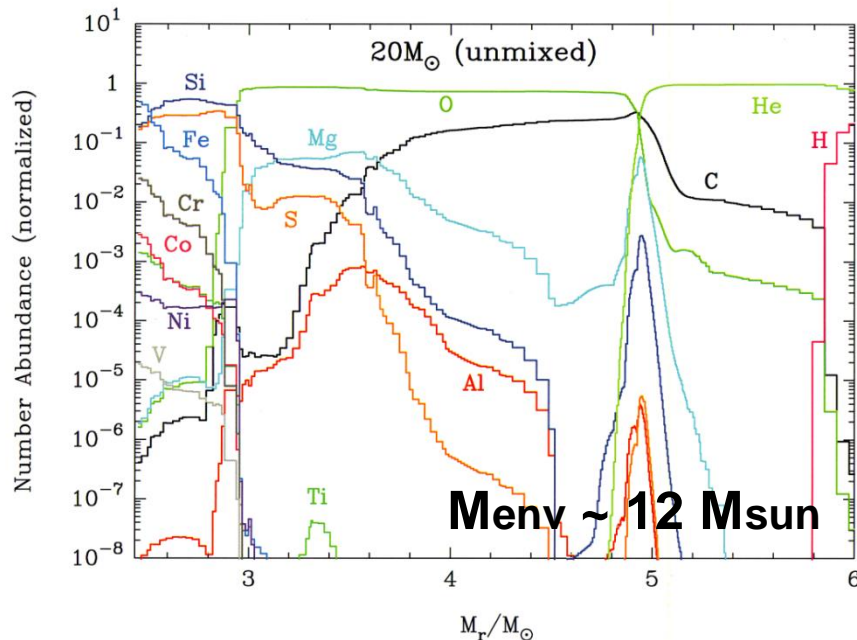
# 2-2. Dust formation in primordial SNe

Nozawa+03, ApJ, 598, 785

- nucleation and grain growth theory (Kozasa & Hasegawa 1988)
- no mixing of elements within the He-core
- complete formation of CO and SiO, sticking probability=1

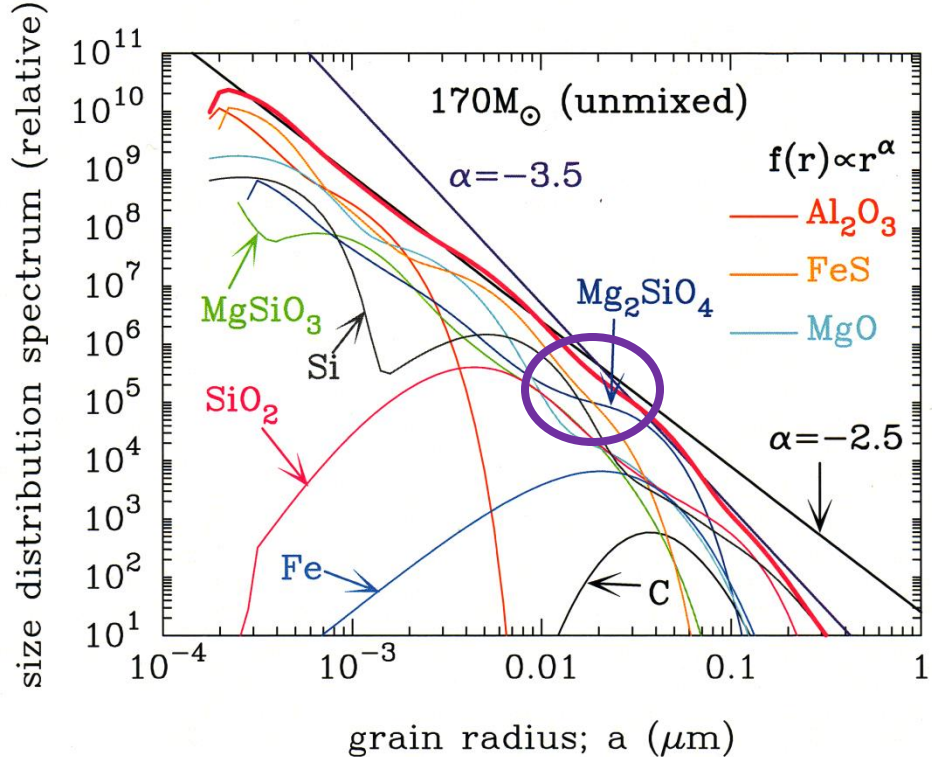
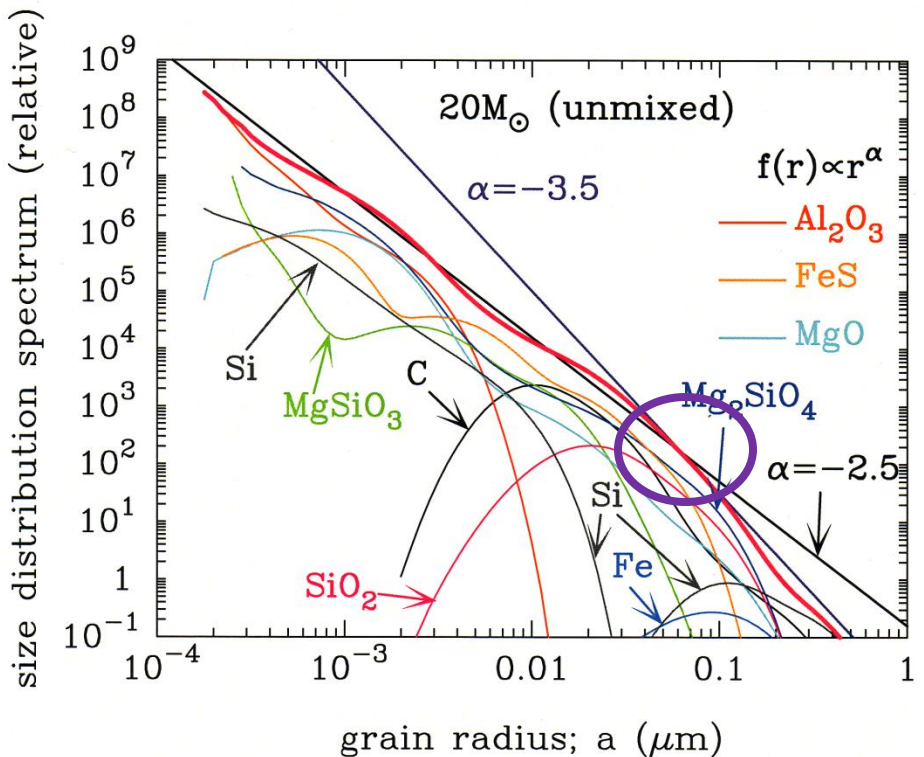
## ○ Population III SNe model (Umeda & Nomoto 2002)

- SNe II-P :  $M_{ZAMS} = 13, 20, 25, 30 M_{\text{sun}}$  ( $E_{51}=1$ )
- PISNe :  $M_{ZAMS} = 170 M_{\text{sun}}$  ( $E_{51}=20$ ),  $200 M_{\text{sun}}$  ( $E_{51}=28$ )





# 2-3. Size distribution spectrum of dust



- grain radii range from a few Å up to 1 μm
- average dust radius is smaller for PISNe than SNe II-P

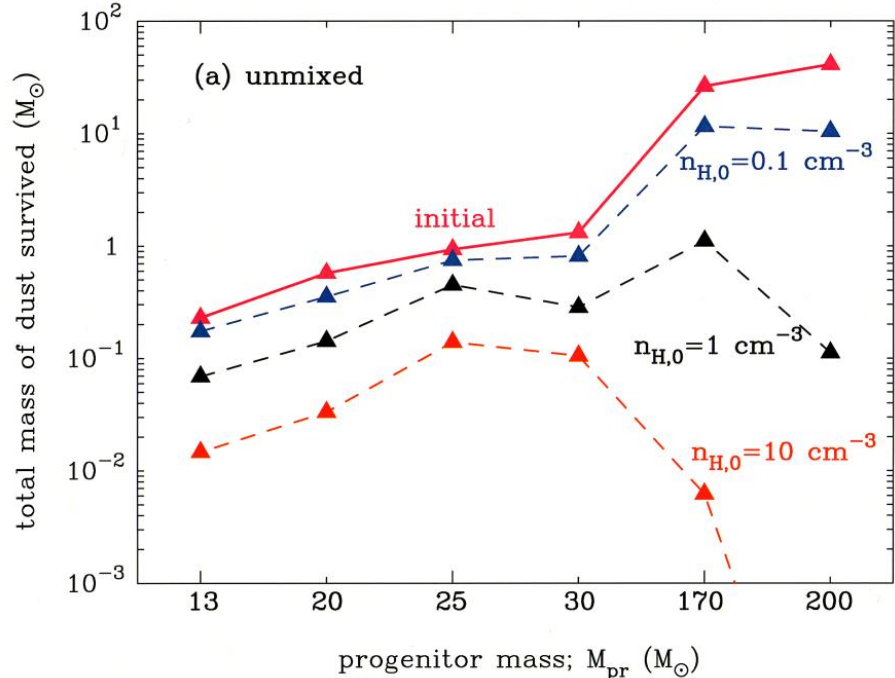
**amount of newly formed dust grains**

**SNe II-P:  $M_{\text{dust}} = 0.1-1 M_{\text{sun}}$ ,  $f_{\text{dep}} = M_{\text{dust}} / M_{\text{metal}} = 0.2-0.3$**

**PISNe :  $M_{\text{dust}} = 20-40 M_{\text{sun}}$ ,  $f_{\text{dep}} = M_{\text{dust}} / M_{\text{metal}} = 0.3-0.4$**

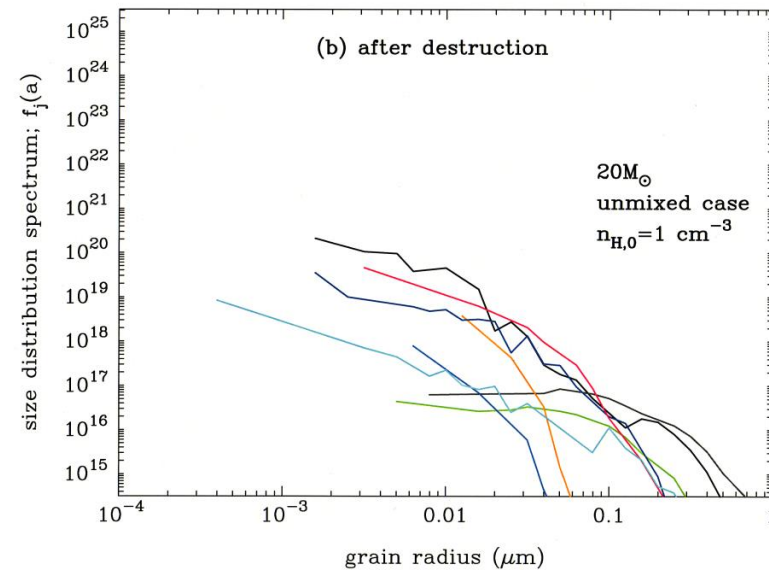
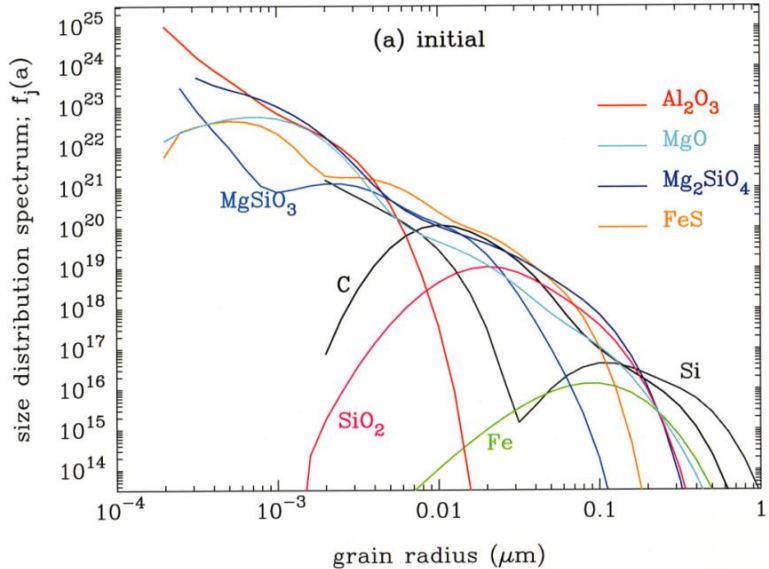
# 2-4. Total mass and size of surviving dust

Nozawa+07, ApJ, 666, 955



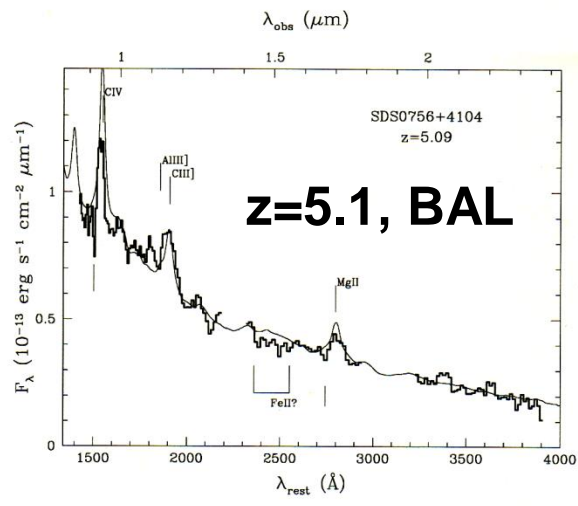
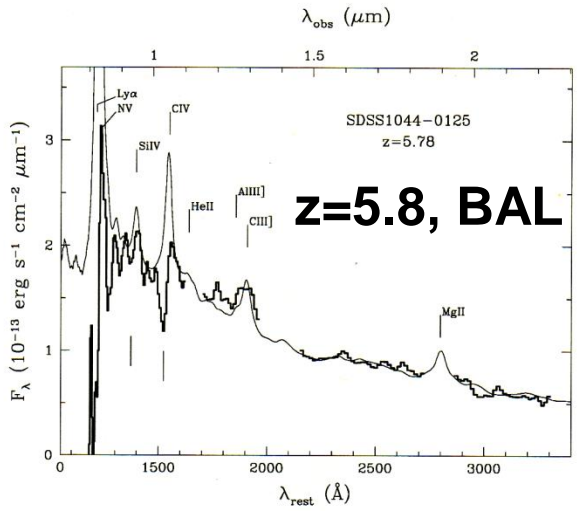
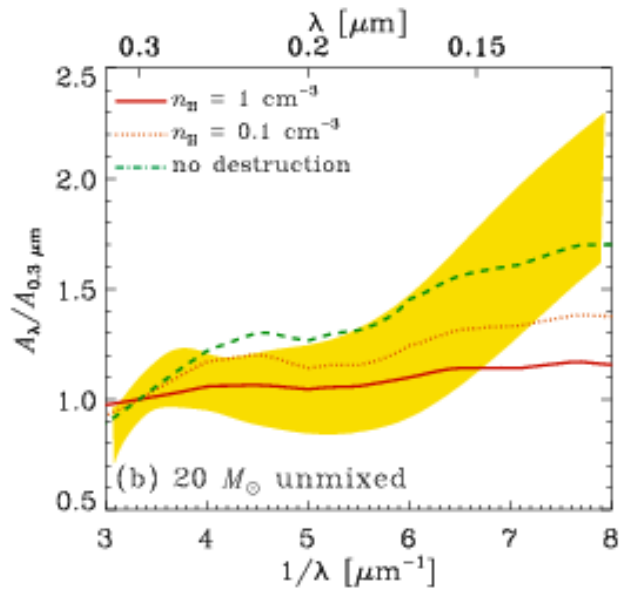
**Total dust mass surviving the destruction in Type II-P SNRs; 0.08-0.8  $M_{\text{sun}}$  ( $n_{H,0} = 0.1-1 \text{ cm}^{-3}$ )**

**Size distribution of surviving dust is dominated by large grains ( $> 0.01 \mu\text{m}$ )**

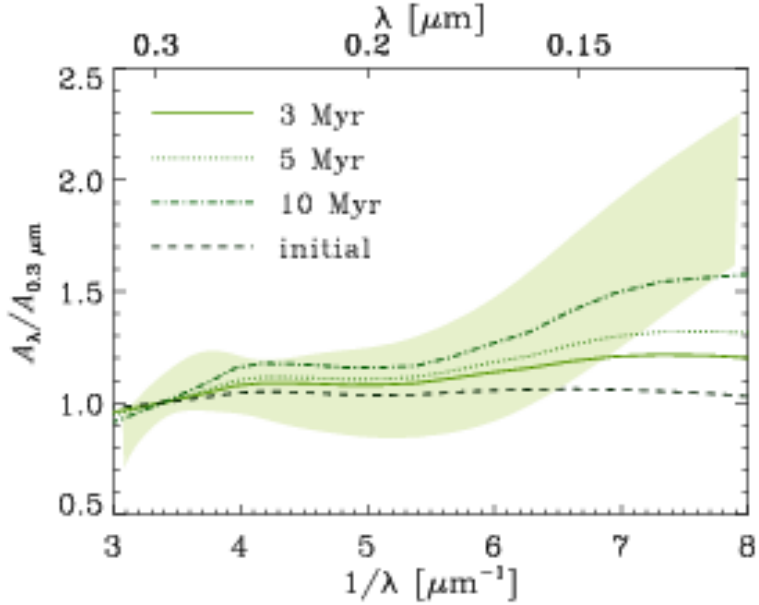
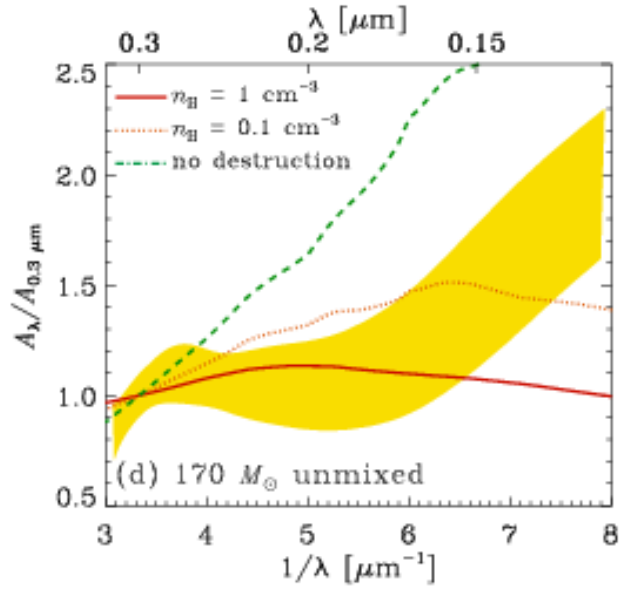


# 2-5. Flattened extinction curves at high-z

Hirashita+08, MNRAS, 384, 1725



Maiolino+04, A&A, 420, 889



Shattering enhances small grains at  $Z=Z_{\text{sun}}$

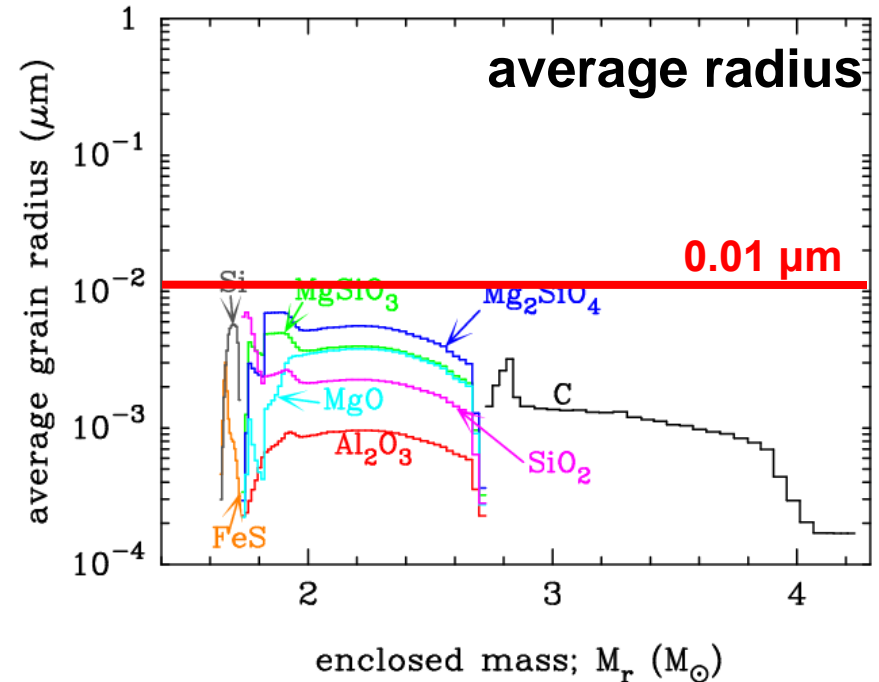
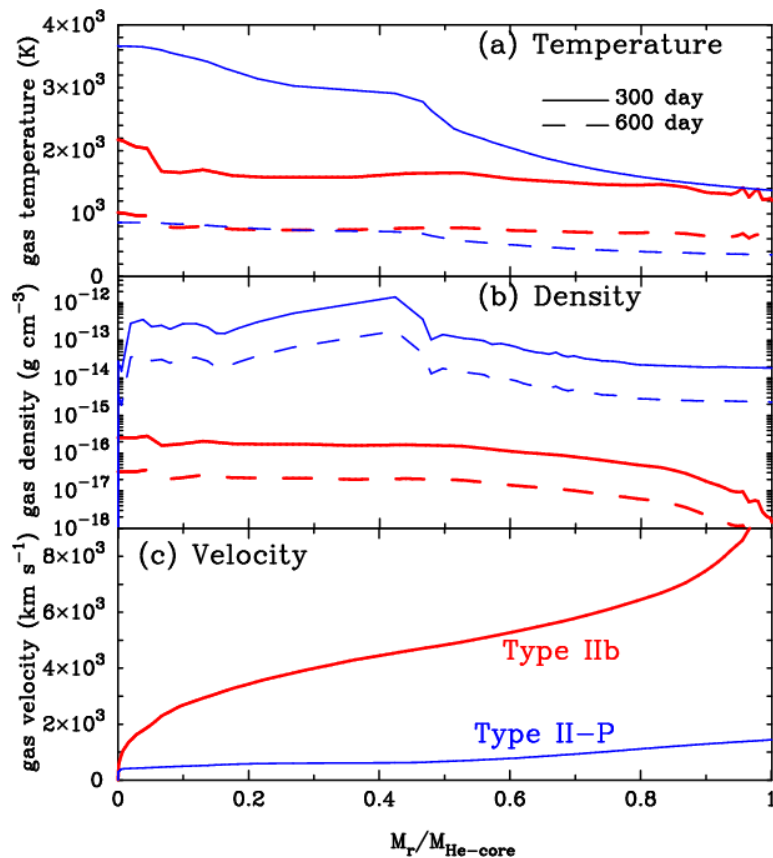
Hirashita+10, MNRAS, 404, 1437

# 2-6. Dust formation in Type IIb SN

Nozawa+10, ApJ, 713, 356

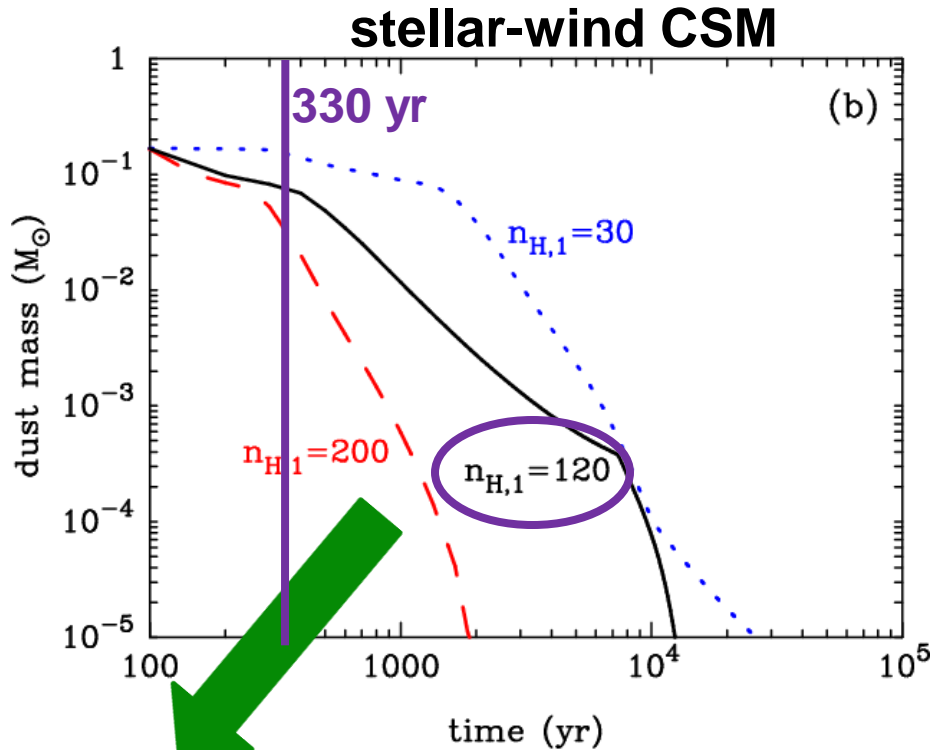
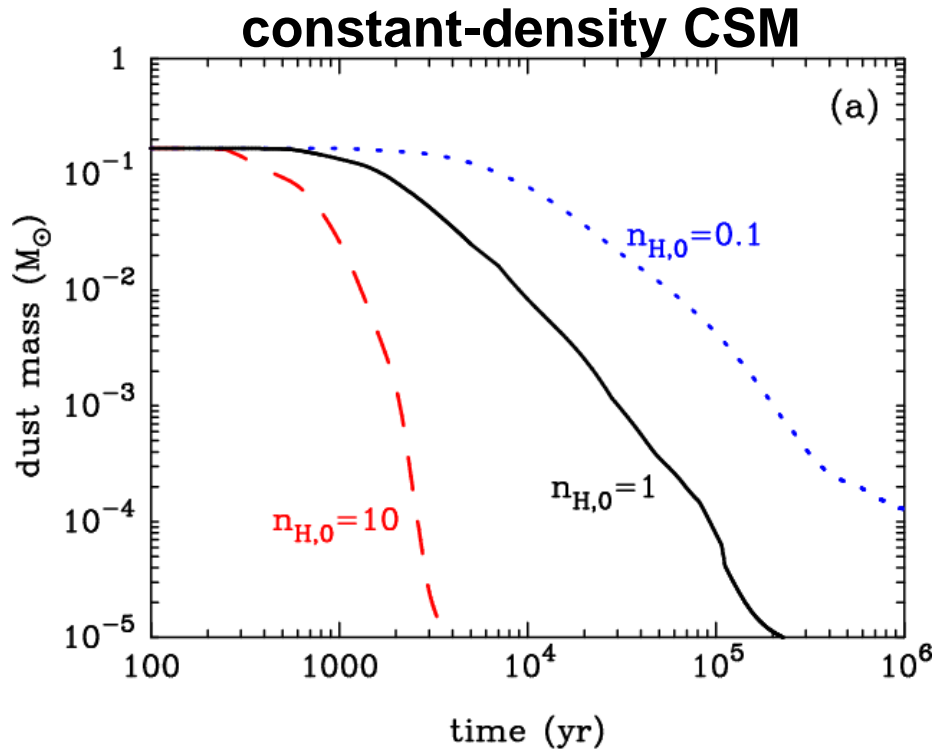
## ○ SN IIb model (SN1993J-like model)

- **MH-env = 0.08 Msun**  
**MZAMS = 18 Msun**  
**Meje = 2.94 Msun**
- $E_{51} = 1$ ,  $M(^{56}\text{Ni}) = 0.07 \text{ Msun}$



- **SN IIb without massive H-env  $\rightarrow a_{\text{dust}} < 0.01 \mu\text{m}$**
- **SN II-P with massive H-env  $\rightarrow a_{\text{dust}} > 0.01 \mu\text{m}$**

# 2-7. Destruction of dust in Type IIb SNR



total mass of dust formed :  $0.167 M_{\text{sun}}$

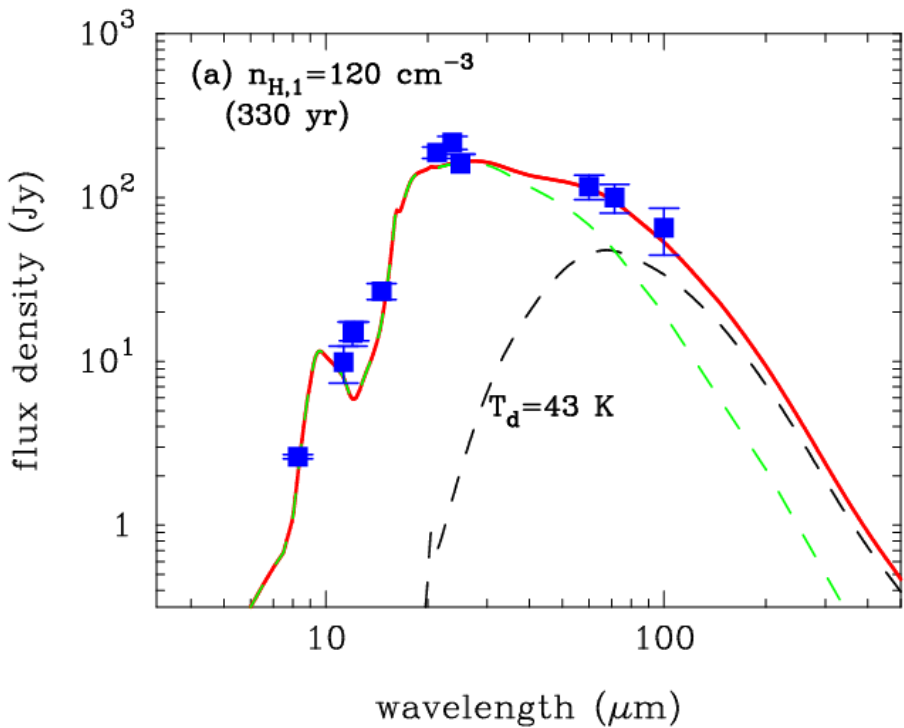
$n_{\text{H},1} = 30, 120, 200 / \text{cc}$   
 $\rightarrow dM/dt = 2.0, 8.0, 13 \times 10^{-5} M_{\text{sun}}/\text{yr}$  for  $v_w = 10 \text{ km/s}$

Almost all newly formed grains are destroyed in shocked gas within the SNR for CSM gas density of  $n_{\text{H}} > 0.1 / \text{cc}$

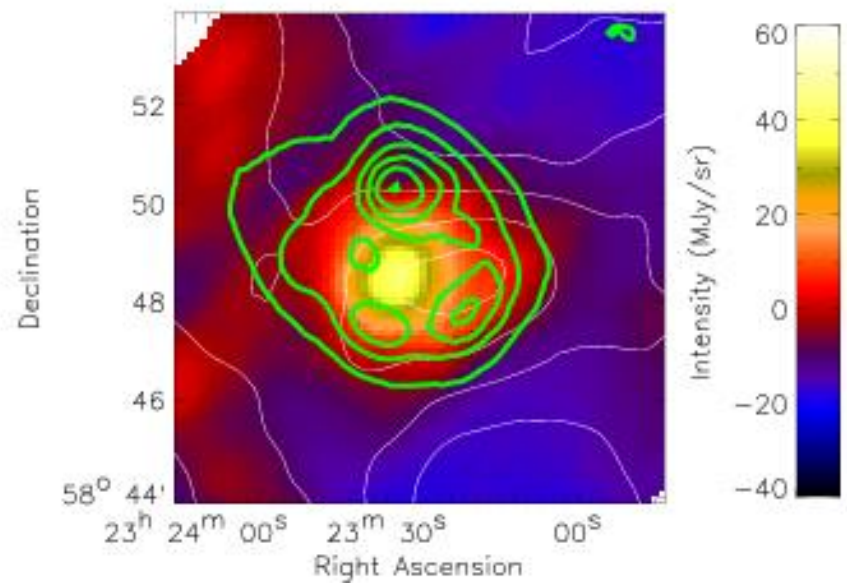
- $\rightarrow$  small radius of newly formed dust
- $\rightarrow$  early arrival of the reverse shock at the He core



# 2-8. Comparison with observations of Cas A



Sibthorpe+09 (arXiv:0910.1094)



**observed IR SED can be well reproduced !**

↑

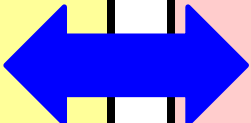
- **$M_{d,warm} \sim 0.008 M_{sun}$**
- **$M_{d,cool} \sim 0.072 M_{sun}$  with  $T_{dust} \sim 40 K$**

**AKARI reduced 90 $\mu$ m image**

→ **centrally peaked cool dust component**

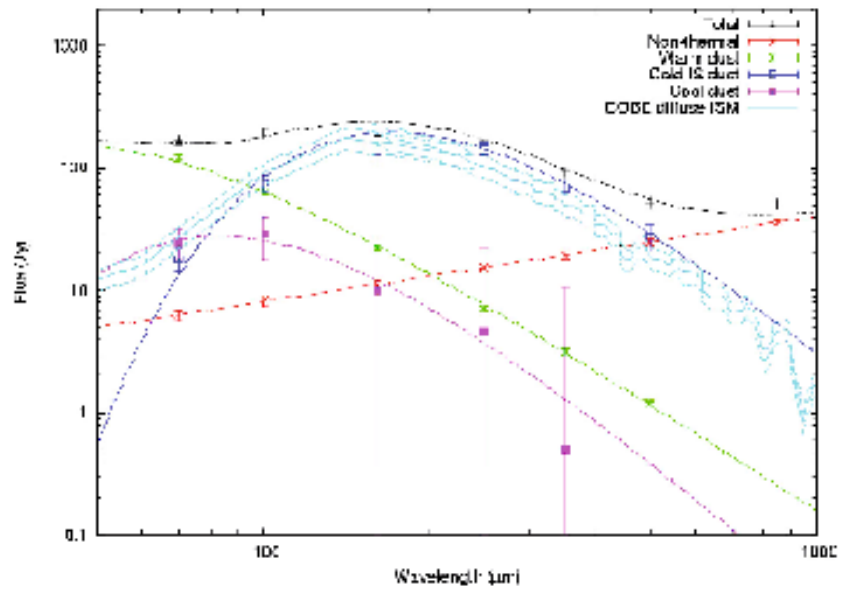
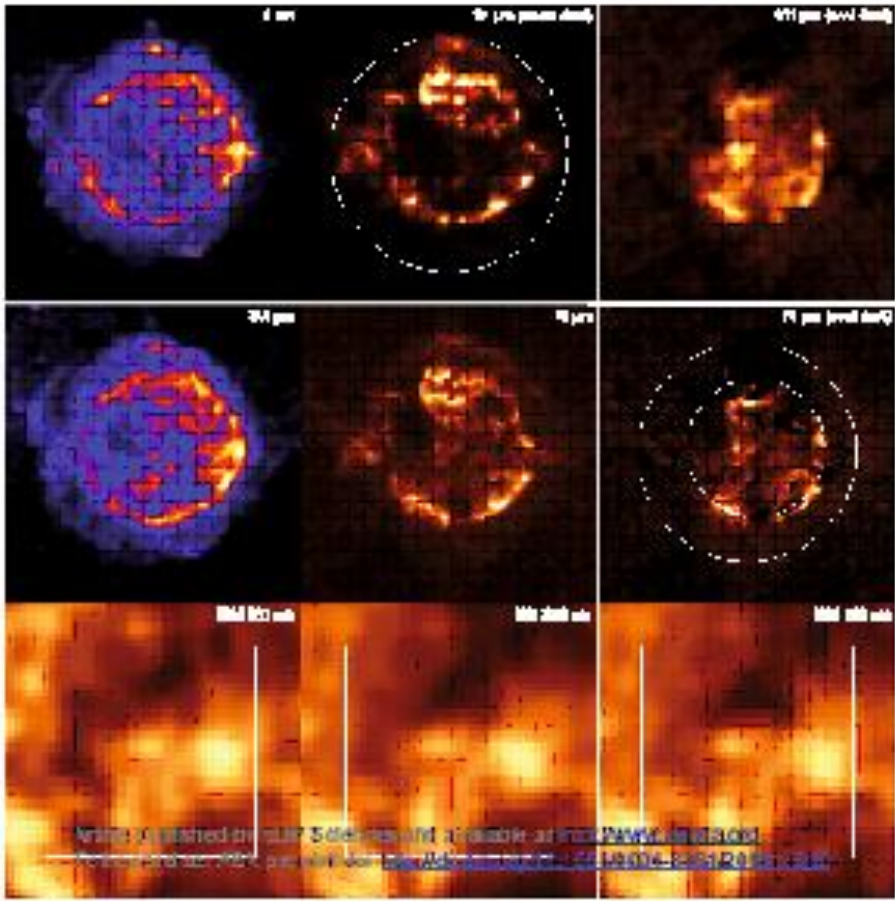
↓

**$M_{d,cool} = 0.03-0.06 M_{sun}$  with  $T_{dust} = 33-41 K$**



# 2-9. Herschel observations of Cas A

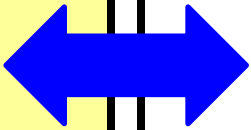
Barlow+10, A&A, 518, L138



confirmation of a cool dust component emitting at 70-160  $\mu\text{m}$  inside reverse shock



- $M_{d,warm} \sim 0.008 M_{sun}$
- $M_{d,cool} \sim 0.072 M_{sun}$  with  $T_{dust} \sim 40 K$



$M_{d,cool} = 0.075 M_{sun}$   
 $T_d \sim 35 K$



## 2-10. Conclusion remarks

- **Type II SNe and PISNe**

  - Average grain radii are larger than  $0.01 \mu\text{m}$

  - **primordial SNe may be important sources of dust**

- **Type IIb, Type Ib/Ic, and Type Ia SNe**

  - Average grain radii are smaller than  $0.01 \mu\text{m}$

  - **envelope-stripped SNe may not be major sources of dust**

- **Extinction curves in the early universe are expected to be flat**

- **Model of dust destruction in Type IIb SNR can well reproduce the observed SED of Cas A**

## **3. Critical metallicity**

# 3-1. Critical metallicity

First (Pop III) star : very massive  $> 10\text{-}100 M_{\text{sun}}$

→ when low-mass population II stars can form?

## • Atomic cooling

–  $Z \sim 10^{-3.5} Z_{\text{sun}}$

(Bromm+01, MNRAS, 328, 969)

–  $[\text{C}/\text{H}] = -3.5, [\text{O}/\text{H}] = -3.05$

(Bromm & Loeb 2003, Nature, 425, 812)

– extending to  $[\text{C}, \text{O}, \text{Si}, \text{Fe}/\text{H}]$

(Santoro & Shull 2006, ApJ, 643, 26)

–  $Z > 10^{-3} Z_{\text{sun}}$  (numerical simulation)

(Smith+07, 661, L5)

–  $Z \sim 10^{-3.5} Z_{\text{sun}}$  (cooling by molecules)

(Jappsen+09, ApJ, 696, 1065)

# 3-2. Minimum stellar metallicity

Frebel+09,  
MNRAS, 392, L50

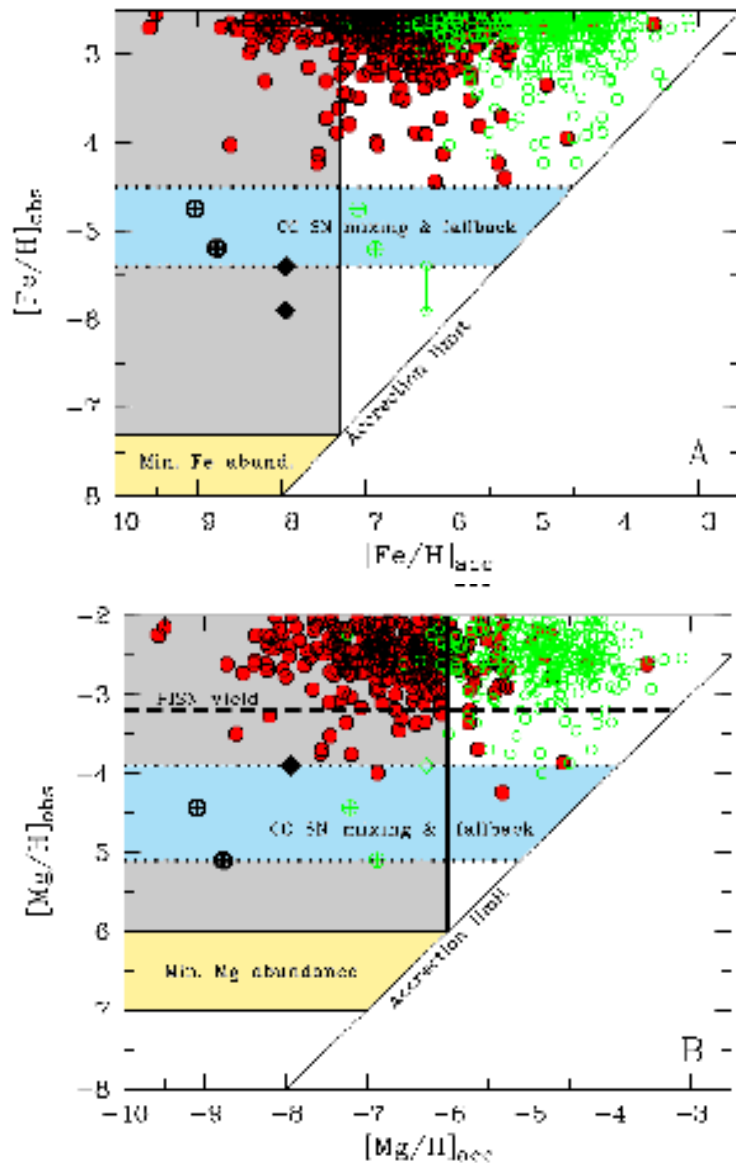


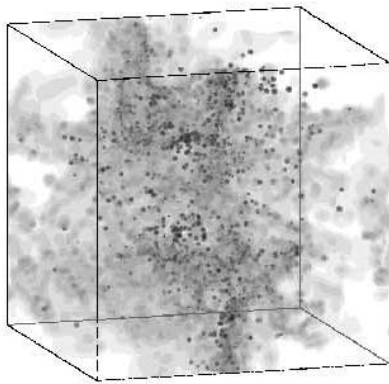
**Figure 1.** Observed vs. “accreted” Fe (*panel A*) and Mg (*panel B*) abundances for the sample of metal-poor stars (*red circles*). The case where all stars pass through a dense cloud once is also presented (*green open circles*). The three most Fe-poor stars are indicated (*crossed circles, diamond*). For HE 1327–2326, both the 1D non-LTE and 3D LTE Fe values are shown. All stars have accreted fewer metals than what is observed, thus demonstrating the validity of the basic assumption underlying stellar archaeology. The minimum Fe and Mg abundance ranges, calculated under the assumption of a top-heavy Pop III IMF, are given (*yellow region*). The approximate Mg abundance arising from a PISN event in an atomic cooling halo is indicated (*dashed line, panel B*), as well as the Fe and Mg levels of enrichment from a  $25 M_{\odot}$  mixing and fallback SN (*dotted lines, blue regions*). We highlight those stars (*gray regions*) that can be used to place constraints on the Pop III IMF, where accretion does not affect whether they lie above or below the theoretical “bedrock abundances”, predicted for a top-heavy IMF. Since all observed Mg abundances within the IMF-sensitive (*gray*) region to date fall above this bedrock range, we conclude that a top-heavy IMF is favored for the first stars.

# 3-3. Thermal evolution of gas clouds

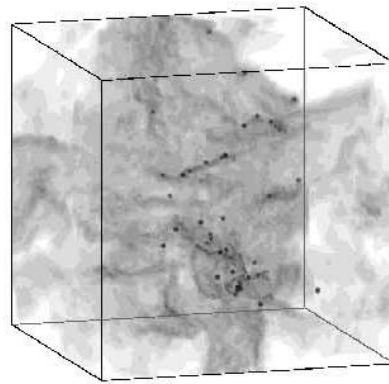
Effective ratio of specific heat

$$\gamma := d \log p / d \log \rho$$

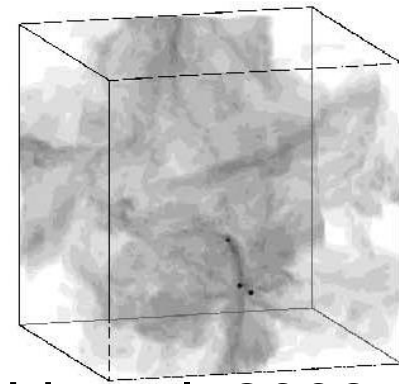
$$\gamma = 0.2$$



$$\gamma = 1 \text{ (isothermal)}$$



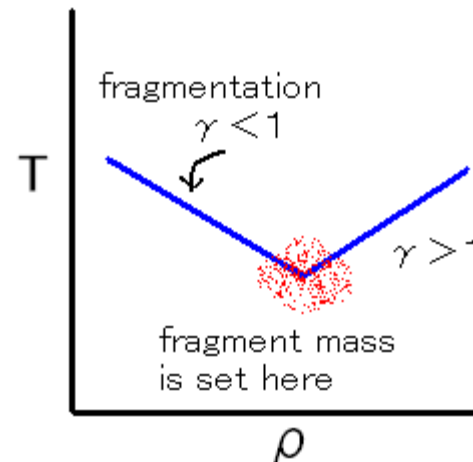
$$\gamma = 1.3$$



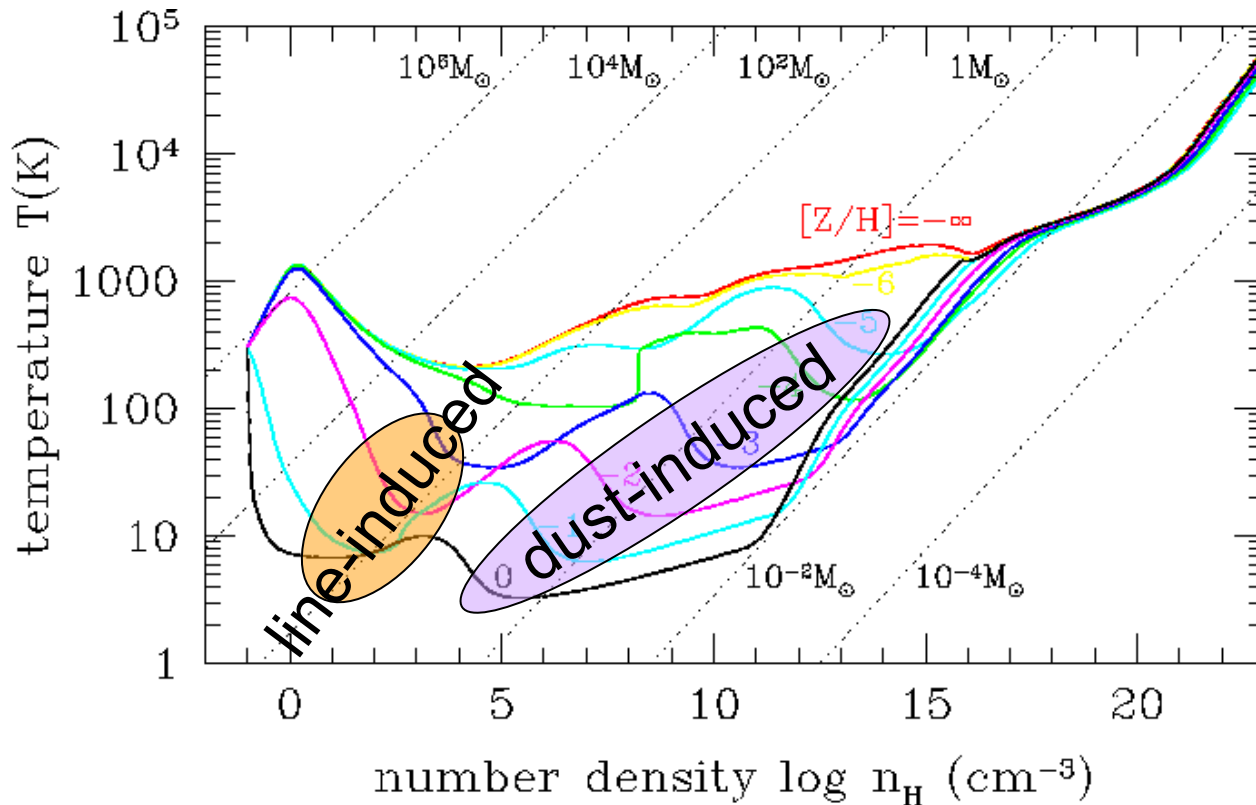
Li et al. 2003

- $\gamma < 1$  vigorous fragmentation,
- $\gamma > 1$  fragmentation suppressed
- The Jeans mass at  $\gamma \sim 1$  (T minimum) gives the fragmentation scale.

$$M_{\text{frag}} = M_{\text{Jeans}} @ \gamma = 1$$



# 3-4. Thermal evolution of gas clouds



Omukai+05,  
ApJ, 626, 627

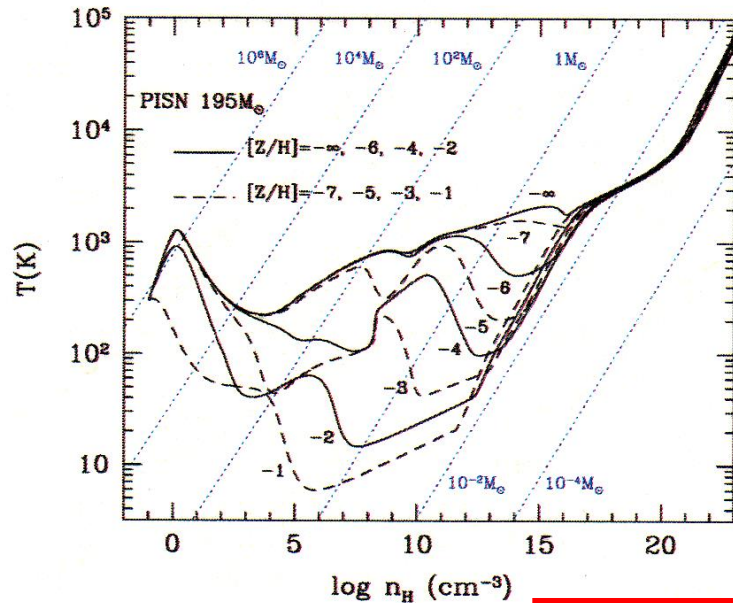
- one-zone model
- dust model :  
Pollack+94
- dust/metal ratio :  
same as local ISM

- Dust cooling causes a sudden temperature drop at high density where  $M_{\text{Jeans}} \sim 0.1 M_{\text{sun}}$ , which induces low-mass fragmentation
- low-mass fragments are formed only in the dust-induced mode

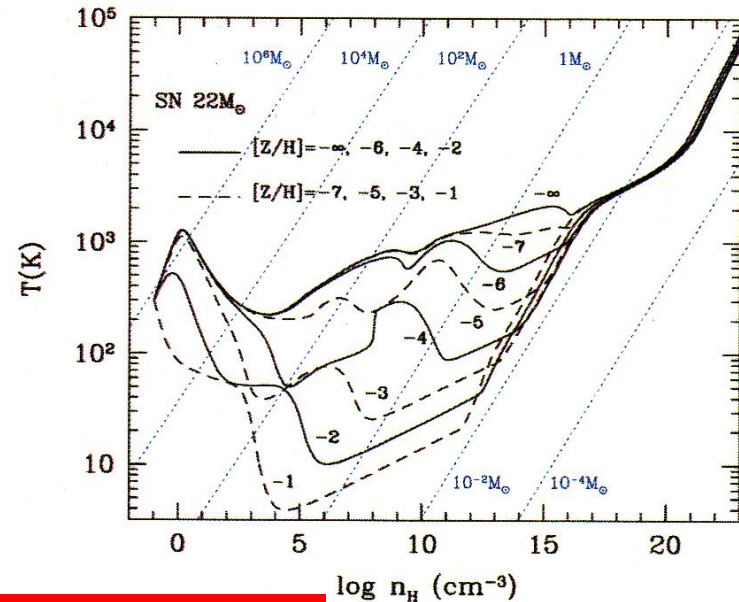
# 3-5. Dust from the first stars

Schneider+06, MNRAS, 369, 1437

progenitor: PISNe (195 M<sub>sun</sub>)



progenitor: SN II (22 M<sub>sun</sub>)



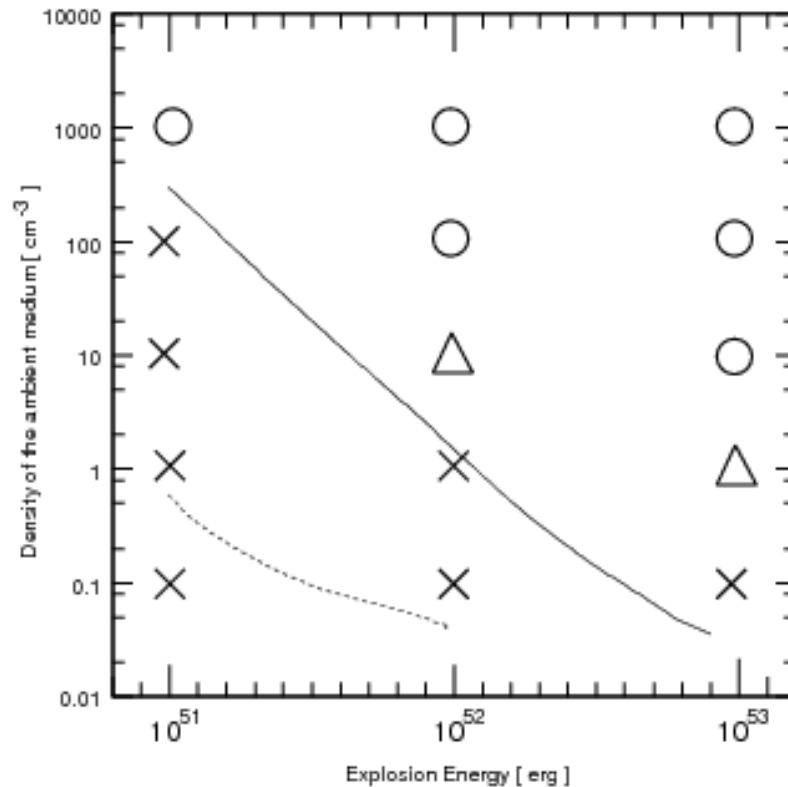
$$Z_{cr} \sim 10^{-6} Z_{sun}$$

## Dust from SNe

- larger area per unit dust mass (smaller radius)
- more refractory composition (silicates, amorphous carbon)



# 3-6. Fragmentation of SN shell



**Nagakura+09, MNRAS,  
399, 2183**

**Figure 8.** Dependence of the fragmentation result of the shell on the ambient density and explosion energy for metallicities  $Z = 10^{-2}Z_{\odot}$  and  $Z = 10^{-4}Z_{\odot}$ . In the cases of  $E_{\text{SN}} = 10^{51}$  and  $10^{52}$  erg, the circles, triangle, and crosses mean that the fragmentation occurs for both metallicities, only for  $Z = 10^{-2}Z_{\odot}$ , and for neither, respectively. In the cases of  $E_{\text{SN}} = 10^{53}$  erg, the circles and crosses represent the successes and fails of the fragmentation respectively, and the triangle satisfies the condition (10) but does not equation (11). Also plotted are the results by Salvaterra et al. (2004; solid) and Machida et al. (2005; dotted), above which the fragmentation occurs.

# 3-7. CMB can affect fragmentation mass

Schneider+10, MNRAS, 369, 1437

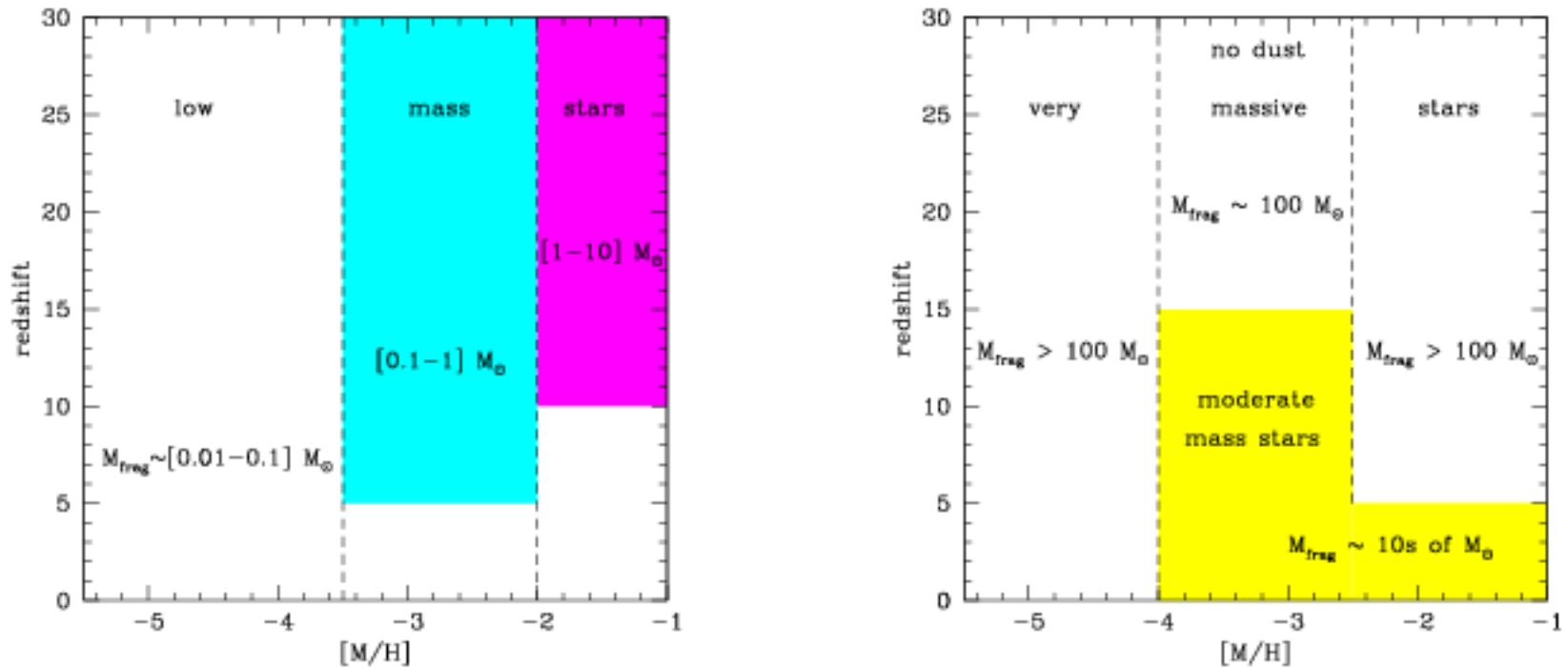


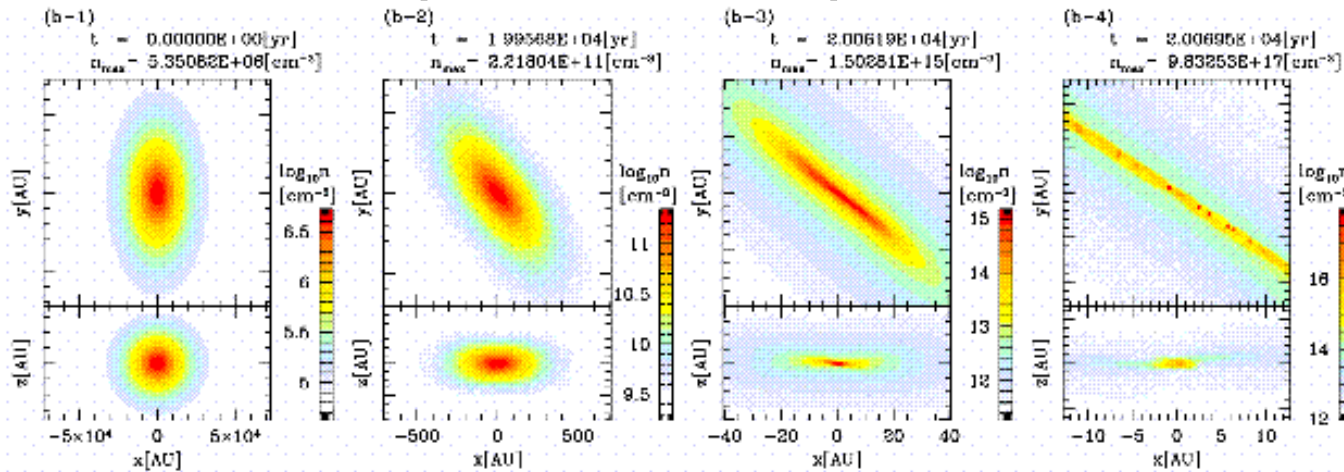
**Figure 4.** Schematic representation of the characteristic masses associated to the relevant fragmentation regimes in the metallicity-redshift plane. In the left panel, we report only the typical scales associated to dust-induced fragmentation, since line-induced fragmentation leads to masses  $> 50M_{\odot}$  independent of the initial metallicity or redshift. In the right panel, we show the scales expected in models with no dust (see text).

# 3-8. 3D-simulation of cloud fragmentation (1)

Tsuribe & Omukai 2005, 642, L61

Tsuribe & Omukai 2008, 676, L45

$[M/H] = -5.5$  ( $Z = 3 \times 10^{-6} Z_{\text{sun}}$ )



▪  $\rho$ - $T$  evolution given by one-zone model for PISN-dust

$Z > \sim 10^{-6} Z_{\text{sun}}$

→ long filament forms during dust-cooling phase

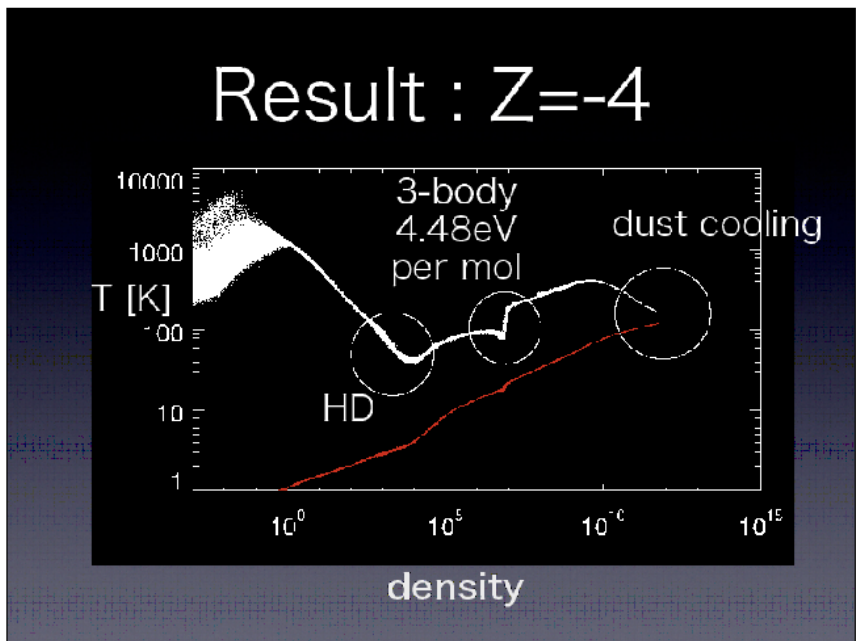
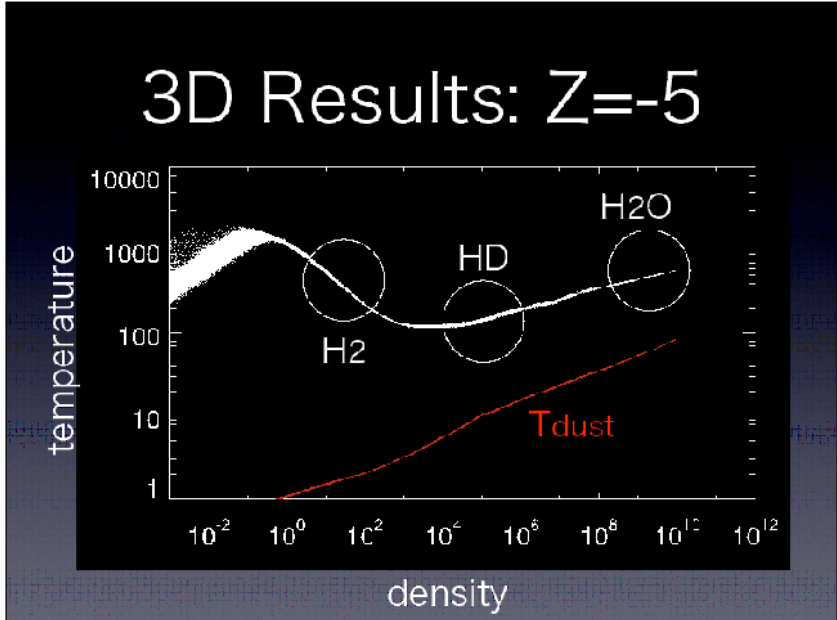
→ fragmentation into low-mass ( $0.1$ - $1 M_{\text{sun}}$ ) objects

$Z_{\text{cr}} \sim 10^{-6} - 10^{-5} Z_{\text{sun}}$

# 3-9. 3D-simulation of cloud fragmentation (2)

**Yoshida (2010)**

- $Z = 10^{-5} Z_{\text{sun}}$   
No fragmentation
- $Z = 10^{-4} Z_{\text{sun}}$   
**fragmentation**  
fragment mass  $\sim 0.1 M_{\text{sun}}$



## Fragmentation

5AU

Fragment mass  $\sim 0.1 M_{\text{sun}}$

Speculation: low-Z subsolar mass stars at high-z

## 3-10. Concluding remarks

- **Critical metallicity (induced by dust) is likely to be  $Z = 10^{-6}$  to  $10^{-4} Z_{\text{sun}}$**

## **4. EMP-stars and dust**

# 4-1. Peculiar abundances of EMP stars

Vankatesan+06, ApJ, 640, 31

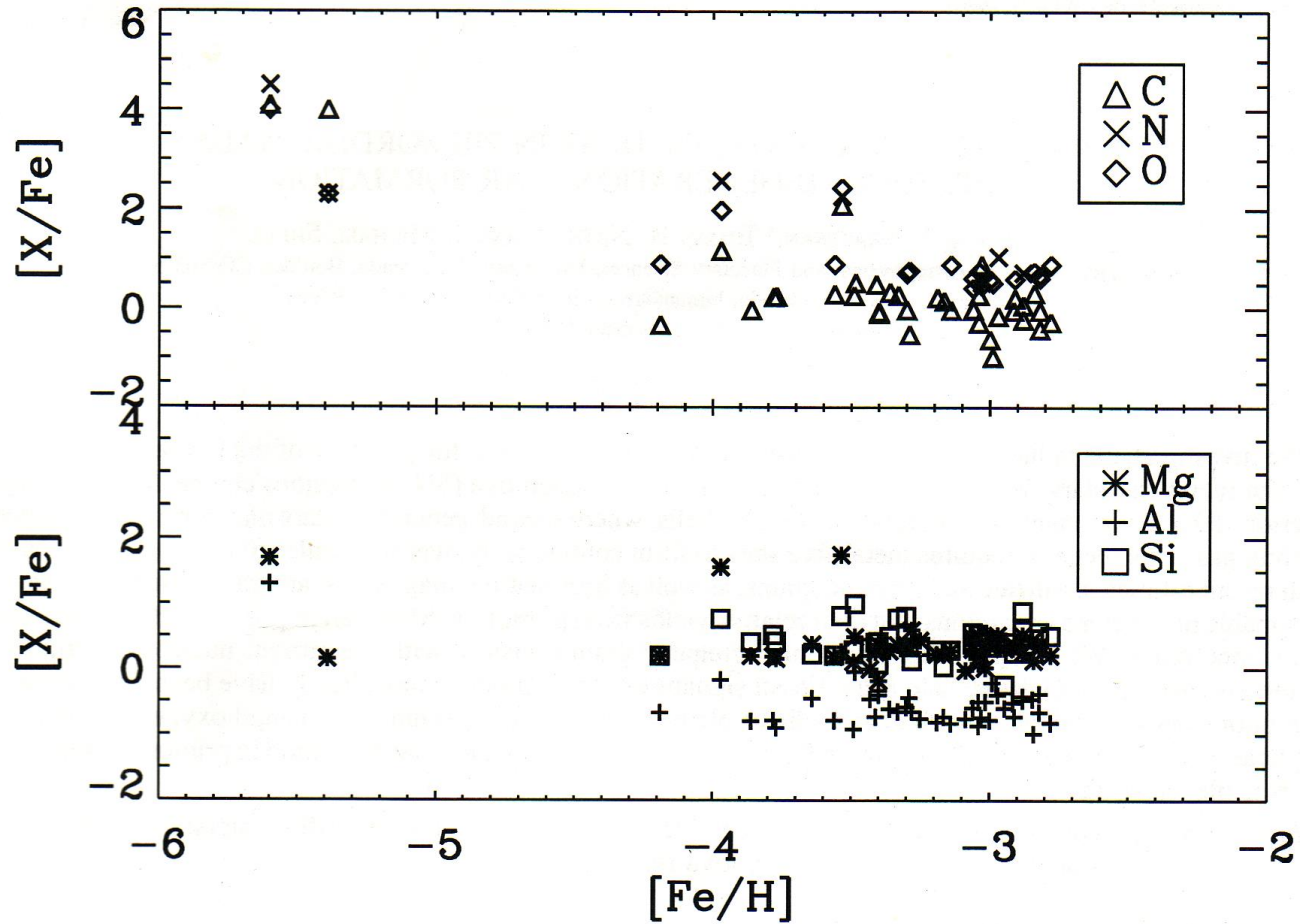


FIG. 1.—Observed abundances of (top) C, N, O, and (bottom) Mg, Al, and Si relative to Fe as a function of  $[Fe/H]$  in EMP halo stars. See text for discussion.

# 4-2. Chemically peculiar stars

Venn+08, ApJ, 677, 572

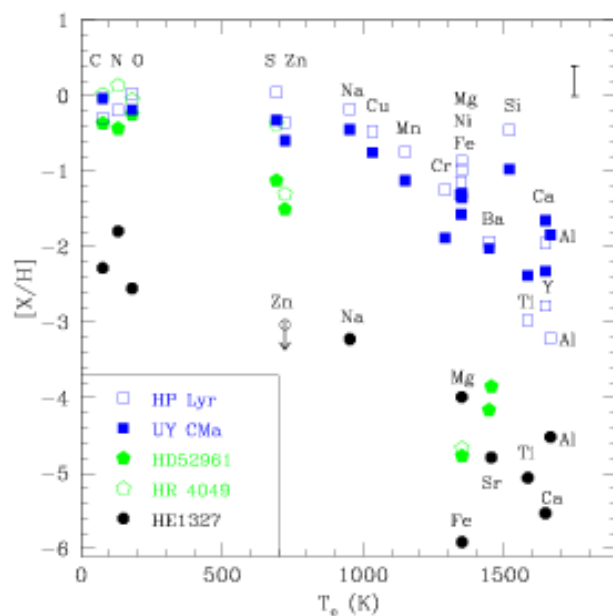


Fig. 2.—  $[X/H]$  abundances in HE1327-2326 from Frebel & Christlieb (2007) against the solar condensation temperatures from Lodders (2003). LTE abundances (solid points) and the upper limit for Zn are shown, all with (3D) corrections for stellar granulation. This abundance pattern is compared to the post-AGB and RV Tauri stars (references in Figure 1). While the abundance pattern for HE1327-2326 resembles those of the chemically peculiar stars, the high  $[Mg/Fe]$  ratio and Al values are striking. Typical errors are  $\leq 0.20$  dex shown by the errorbar in the upper right; Aoki *et al.* (2006) suggest slightly larger errors for C and N in HE1327-2326, of 0.24 and 0.30 dex, respectively.

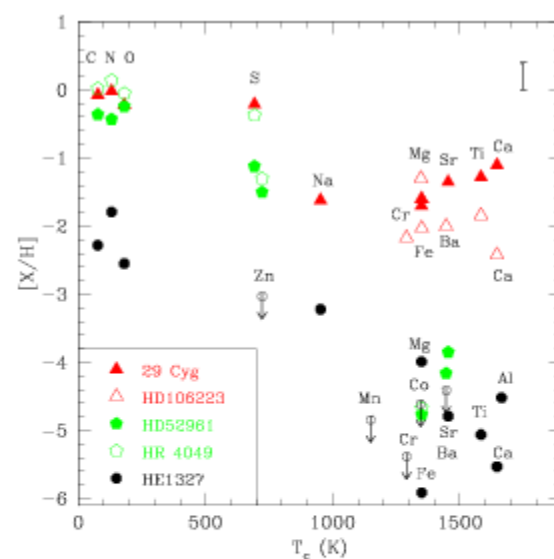


Fig. 3.—  $[X/H]$  abundances in HE1327-2326 from Frebel & Christlieb (2007) as in Figure 2 with additional upper-limits noted. The abundance pattern is compared to the post-AGB stars and two Lambda Bootis stars (29 Cyg from Venn & Lambert 1990, and HD 106223 from Andrievsky *et al.* 2002).

- preferential removal of metals by dust formation
- dilution by the accretion of metal-poor interstellar gas



# 4-3. Radiative transport of dust

Vankatesan+06, ApJ, 640, 31

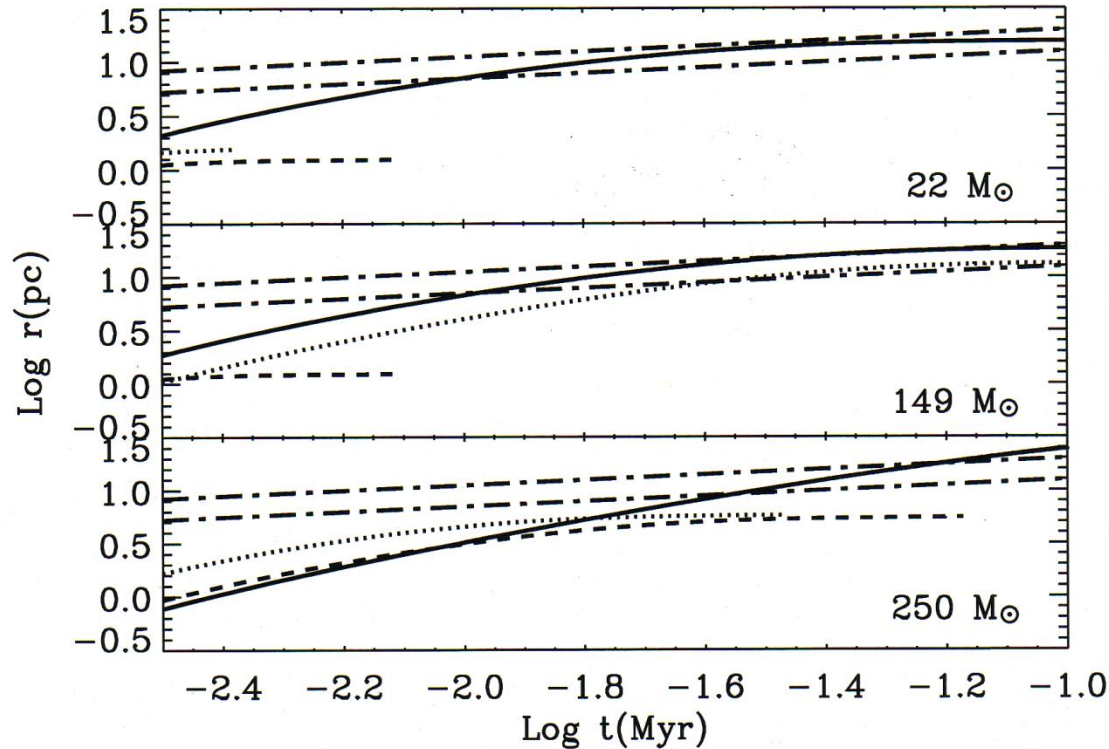


FIG. 4.—Positions of dust grains within SNRs in primordial galaxies, shown as a function of time as they are radiatively transported outward from the center of the SNR. Stellar masses of (top) 22, (middle) 149, and (bottom) 250  $M_{\odot}$  span the range of SN progenitors considered in this work. Solid, dotted, and dashed curves refer to graphites, silicates, and magnetite grains, respectively. The initial grain sizes for the compounds in each panel are detailed in the text. The two dash-dotted lines in each panel describe the adiabatic evolution of the SN shell radius for  $E_{\text{SN}} = 10^{52}$  ergs and ambient gas number densities of (upper line)  $1 \text{ cm}^{-3}$  and (lower line)  $10 \text{ cm}^{-3}$ . See text for discussion.

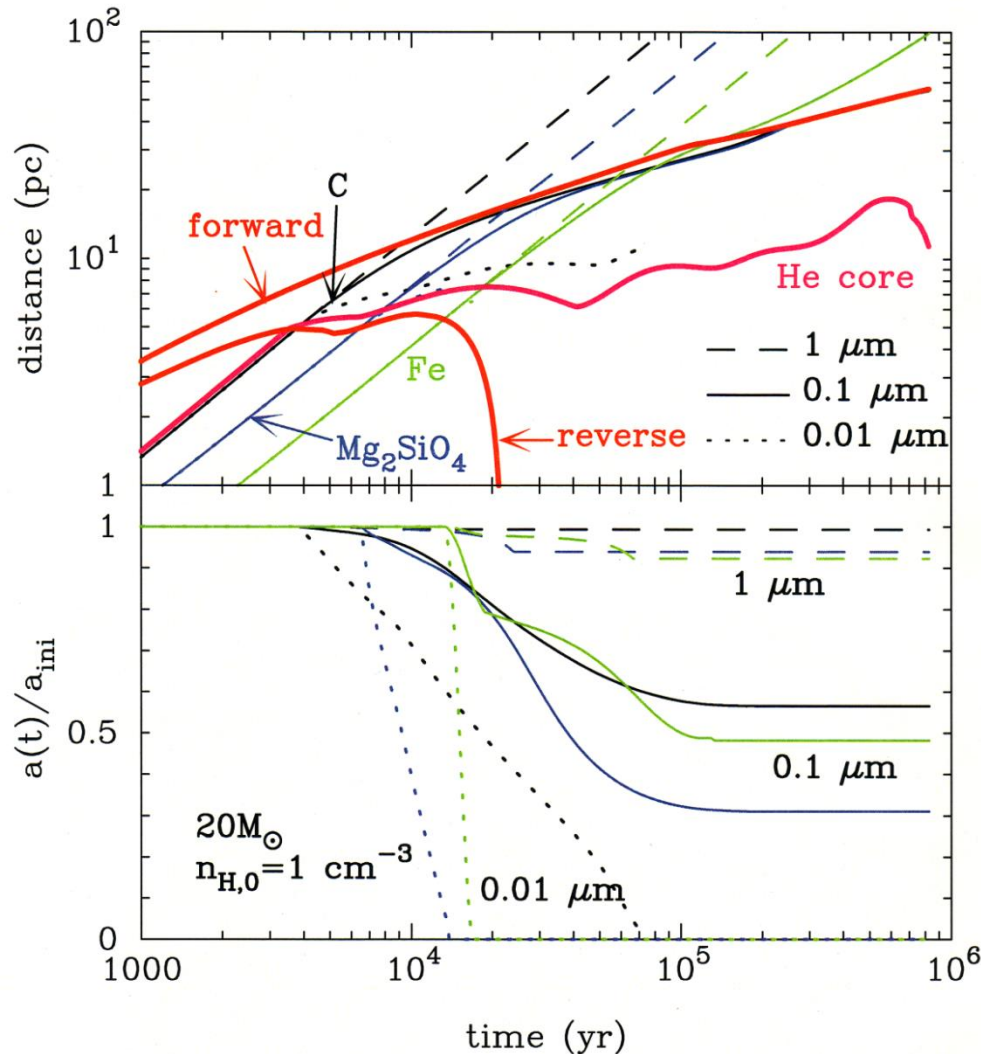
**Dust formed in the first SN is transported to SN shells,  
and some results of segregated grain transport can  
reproduce elemental composition of EMP stars**

# 4-4. Evolution of dust within SNRs

Nozawa+07, ApJ, 666, 955

Model :  $M_{\text{pr}} = 20 M_{\text{sun}}$  ( $E_{51} = 1$ ),  
 $n_{\text{H},0} = 1 \text{ cm}^{-3}$

The evolution of dust heavily depends on the initial radius and chemical composition



- $a_{\text{ini}} = 0.01 \mu\text{m}$  (dotted)  
→ completely destroyed
- $a_{\text{ini}} = 0.1 \mu\text{m}$  (solid)  
→ trapped in the shell
- $a_{\text{ini}} = 1 \mu\text{m}$  (dashed)  
→ injected into the ISM

# 4-5. Elemental abundance in the SNR shell (1)

$M_{pr}$ ( $M_{\odot}$ )	[Fe/H]	[C/Fe]	[O/Fe]	[Mg/Fe]	[S/Fe]	metallicity of shell $Z > Z_{cr} = 10^{-6} Z_{\odot}$		$\log(Z/Z_{\odot})$
$n_{H,0} = 0.1 \text{ cm}^{-3}$								
13	-6.43	-0.274	-0.699	-0.230	1.92	-2.60	0.239	-5.89
20	-5.20	0.117	-0.595	0.034	0.410	-1.97	0.242	-5.44
25	-5.90	1.11	-1.42	-0.500	-0.552	-0.563	0.242	-5.55
30	-5.56	0.566	-0.043	0.739	0.866	0.905	0.242	-5.33
$n_{H,0} = 1 \text{ cm}^{-3}$								
13	-5.15	1.11	-0.555	-0.459	1.01	-	-2.18	-4.72
20	-5.53	0.992	0.585	1.16	1.87	-	0.200	-4.68
25	-5.23	1.09	-0.412	0.407	0.989	-	0.241	-4.79
30	-5.11	0.797	0.242	1.09	1.26	-5.72	0.242	-4.60
$n_{H,0} = 10 \text{ cm}^{-3}$								
13	-4.13	[Fe/H] = -5.62 (HE0107-5240; Collet et al. 2006)						-4.40
20	-4.92	[Fe/H] = -5.96 (HE1327-2326; Frebel et al. 2008)						-4.09
25	-5.10	[Fe/H] = -4.75 (HE0557-4840; Noris et al. 2007)						-3.91
30	-5.11	3-D corrected						-3.84

# 4-6. Elemental abundance in the SNR shell (2)

Nozawa+09 (arXiv:0812.1448)

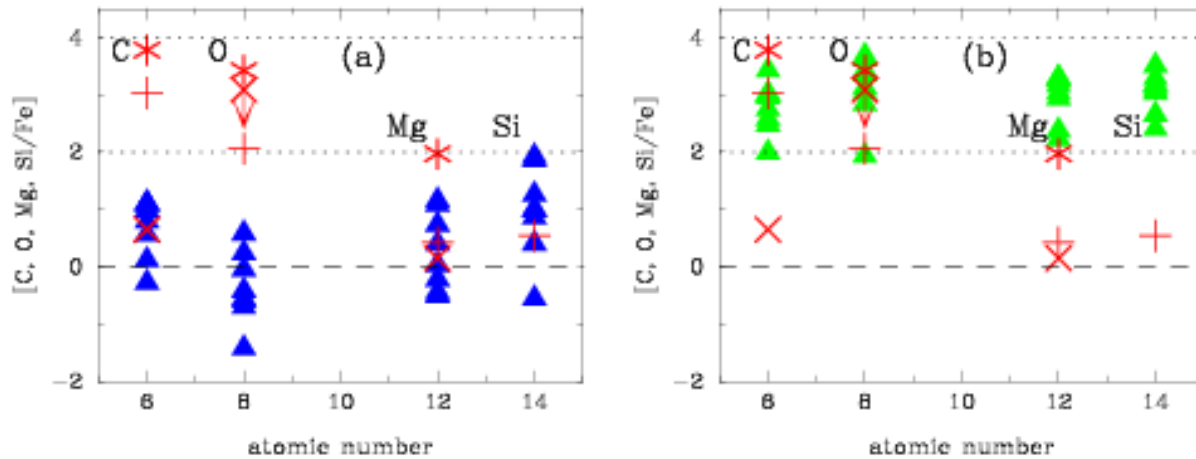


Figure 6. Abundances of C, O, Mg and Si relative to solar value in the dense shell of primordial SN II remnants for  $n_{\text{H},0} = 0.1$  and  $1 \text{ cm}^{-3}$  (filled triangles); (a) derived from the elemental composition of the grains piled up in the shell, and (b) derived from the elemental composition of the piled-up grains and the gas outside the innermost Fe layer. For the observational data of HMP and UMP stars, the 3-D corrected abundances are adopted and are denoted by plus (HE0107–5240 with  $[\text{Fe}/\text{H}] = -5.62$ , Collet et al. 2006), asterisk (HE1327–2326 with  $[\text{Fe}/\text{H}] = -5.96$ , Frebel et al. 2008), and cross (HE0557–4840 with  $[\text{Fe}/\text{H}] = -4.75$ , Norris et al. 2007).

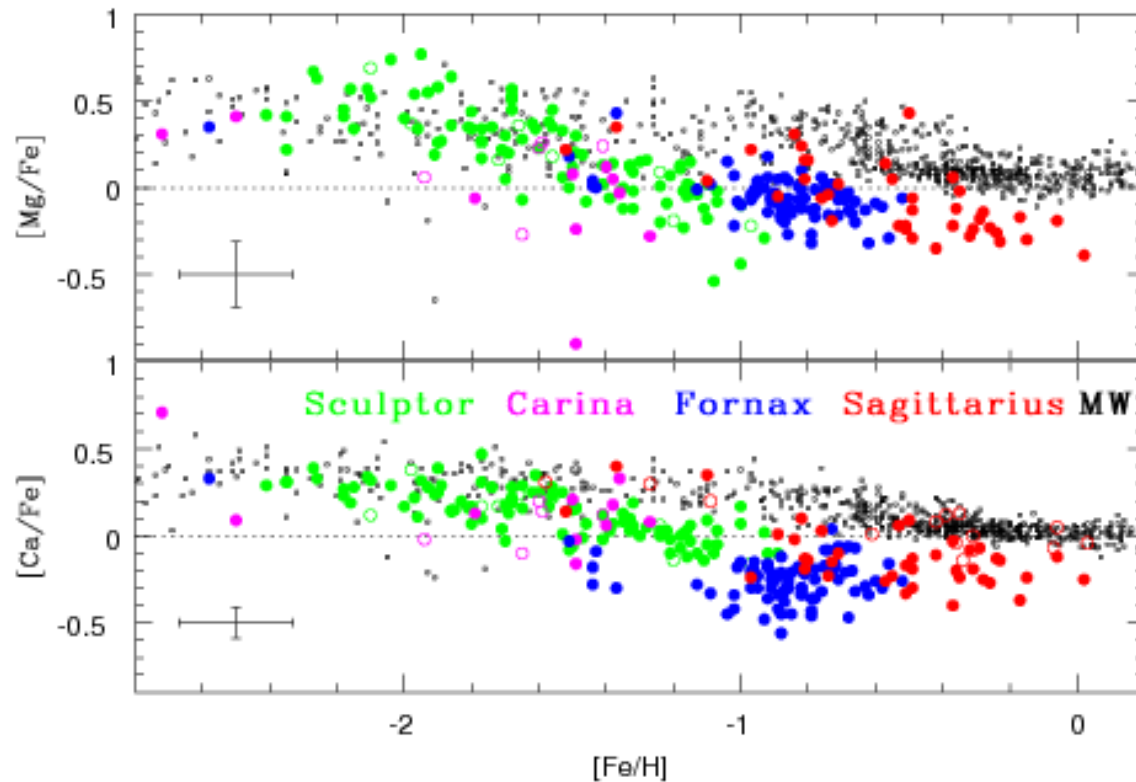
$$\begin{aligned} -6 < [\text{Fe}/\text{H}] < -5 \\ 0 < [\text{Mg}, \text{Si}/\text{Fe}] < 2 \end{aligned}$$

↓  
elemental composition of dust piled up in the shell can reproduce abundance pattern in HMP stars

The transport of dust segregated from metal-rich gas can be responsible for the elemental composition of Population II.5 stars formed in the dense SN shell



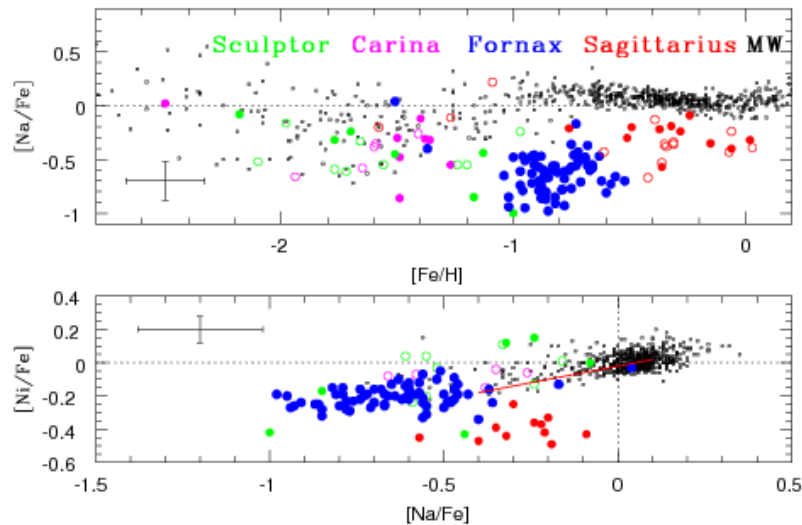
# 4-7. Elemental abundance of dwarf galaxies (1)



**Tolstoy+10,  
ARAA, 47, 371**

Figure 11: Alpha-elements (Mg and Ca) in four nearby dwarf spheroidal galaxies: Sgr (red: Sbordone et al., 2007; Monaco et al., 2005; McWilliam & Smecker-Hane, 2005), Fnx (blue: Letarte, 2007; Shetrone et al., 2003), Scl (green: Hill et al. in prep; Shetrone et al., 2003; Geisler et al., 2005) and Carina (magenta: Koch et al., 2008a; Shetrone et al., 2003). Open symbols refer to single-slit spectroscopy measurements, while filled circles refer to multi-object spectroscopy. The small black symbols are a compilation of the MW disk and halo star abundances, from Venn et al. (2004a).

# 4-8. Elemental abundance of dwarf galaxies (2)



## Tolstoy+10

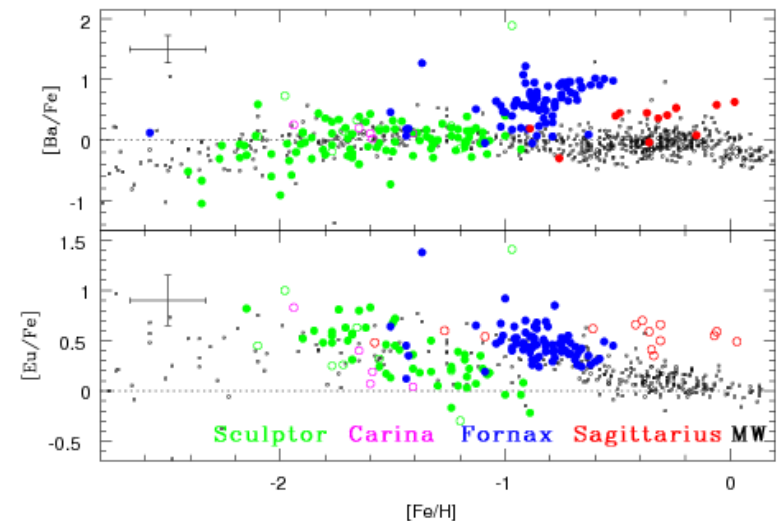


Figure 12: Sodium (above) and nickel (below) in the same four dSphs as in Fig. 11, compared to the MW. Sgr (red: Sbordone et al., 2007; Monaco et al., 2005; McWilliam & Smecker-Hane, 2005), Fnx (blue: Letarte, 2007; Shetrone et al., 2003), Scl (green: Hill et al. in prep; Shetrone et al., 2003; Geisler et al., 2005) and Carina (magenta: Koch et al., 2008a; Shetrone et al., 2003). Open symbols refer to single-slit spectroscopy measurements, while filled circles refer to multi-object spectroscopy. The small black symbols are a compilation of the MW disk and halo star abundances, from Venn et al. (2004a).

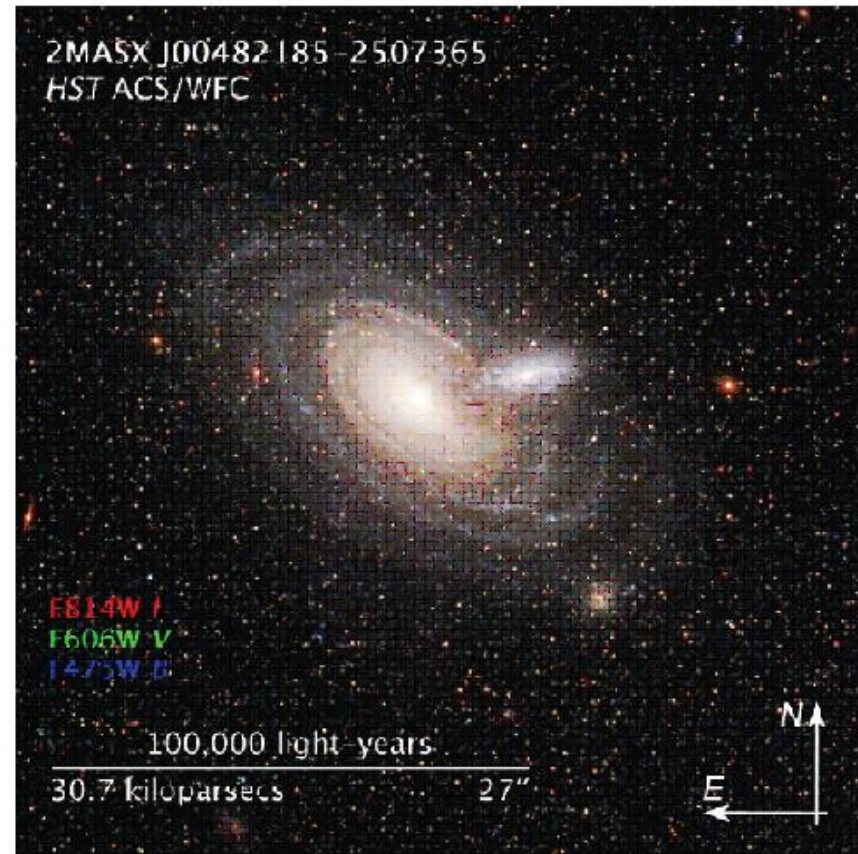
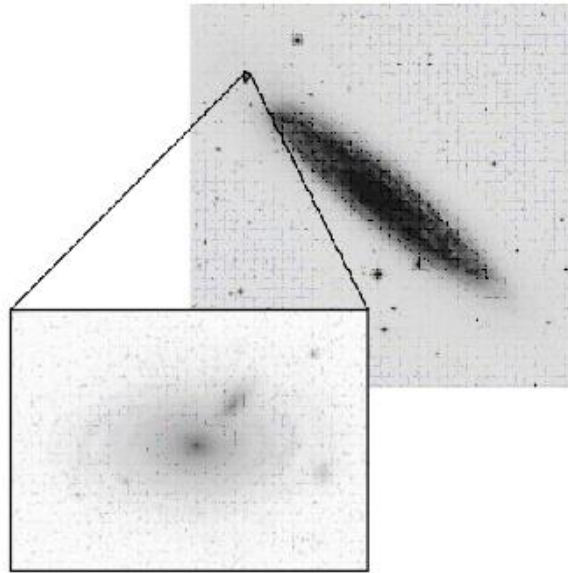
Figure 13: Neutron-capture elements Y, Ba & Eu in the same four dSphs as in Fig. 11, compared to the MW. Sgr (red: Sbordone et al., 2007; Monaco et al., 2005; McWilliam & Smecker-Hane, 2005), Fnx (blue: Letarte, 2007; Shetrone et al., 2003), Scl (green: Hill et al. in prep; Shetrone et al., 2003; Geisler et al., 2005) and Carina (magenta: Koch et al., 2008a; Shetrone et al., 2003). Open symbols refer to single-slit spectroscopy measurements, while filled circles refer to multi-object spectroscopy. The small black symbols are a compilation of the MW disk and halo star abundances, from Venn et al. (2004a).



# 4-9. Confirmation of IGM dust in galaxy halo

ACS Nearby Galaxy Survey Treasury (ANGST)  
Holwerda et al. (2008)

**Menard (2010)**



**How dust grains are transported to the IGM?**

## 4-10. Concluding remarks